Permeability of cementitious materials using a multiscale pore network model

Permeability of Cementitious Materials using a Multiscale Pore Network Model

Saeid Babaei* [(1)a,b,c], Suresh C. Seetharam [(2)b], Arnaud Dizier[(3)d], Gunther Steenackers[(4)c,e] and Bart Craeye[(5)c,f]

[a] SVK N.V., Aerschotstraat 114 B-9100 Sint-Niklaas, Belgium.

[b] Engineered and Geosystems Analysis Unit, Institute for Environment, Health, and Safety, Belgian Nuclear Research Centre (SCK•CEN), Boeretang 200, B-2400 Mol, Belgium.

[c] Faculty of Applied Engineering, University of Antwerp, EMIB Research Group, Groenenborgerlaan 171 - 2020 Antwerpen , Belgium.

[d] EIG, EURIDICE, Belgian Nuclear Research Centre (SCK•CEN), Boeretang 200, B-2400 Mol, Belgium.

[e] Faculty of Applied Engineering, University of Antwerp | Op3Mech Research Group Groenenborgerlaan 171 - 2020 Antwerpen.

[f] Odisse University College, Industrial Services & Technologies, DUBIT Research Unit, Belgium.

(1) Tel: +32 474740440, saeid.babaei@svk.be; saeid.babaei@uantwerpen.be

(2) Tel: +32 14 333208, suresh.seetharam@sckcen.be

(3) Tel: +32 14 332998, arnaud.dizier@euridice.be

(4) Tel: +32 00 000000, gunther.steenackers@uantwerpen.be

(5) Tel: +32 00 000000, bart.craeye@uantwerpen.be

Abstract

This paper presents a new multiscale pore network modelling framework for predicting saturated and unsaturated permeability of OPC-based cementitious materials using a novel algorithmic implementation. The framework fundamentally relies on the data on cement composition and current understanding of cement hydration kinetics and microstructural features. Central to the modelling framework is the ability to numerically estimate pore size distribution (PSD) from existing models and the ability to obtain snapshots of unsaturated microstructure for various degrees of saturation. The framework is an amalgamation of three important existing models: (i) particle packing model for predicting nanoscale PSD, (ii) cement hydration kinetics to estimate microscale PSD, and (iii) a pore network model to estimate the permeability. The proposed pore network modelling is validated against an extensive set of experimental data that includes a very wide range of materials. The predicted intrinsic permeability falls well within the accepted experimental range. Though fewer experimental data are available to compare, the predicted unsaturated permeability shows highly promising results.

1 Introduction

Cementitious materials are ubiquitously used in urbanization. Besides their classical use in construction, these materials are also envisioned for use both as encapsulation of radioactive waste and as engineered barriers for disposal of radioactive waste. One of the major governing parameters for performance and safety assessment of cementitious materials is their permeability because this has a direct link with the transport mechanisms of aggressive substances responsible for degradation of the cementitious matrix. In addition, it is a measure of how the cementitious material can withstand drying due to environmental loading (e.g. atmospheric or heat induced), which can have a decisive impact on shrinkage induced cracks. The intrinsic water permeability, also called specific permeability or absolute permeability, is the measured permeability for a fully saturated state. The unsaturated water permeability or relative permeability is the measured permeability at lower degrees of saturation. However, measuring permeability is not straightforward and there are two main approaches to measure it in laboratory, direct and indirect measurements. While the former is done usually by means of applying a certain pressure gradient or flow rate on a cylindrical sample and quantifying the permeability using Darcy's law, the latter approach involves either the application of a transient pressure pulse technique or the application of poromechanical techniques or inverse analysis of moisture loss experiments. A review of these experimental methods can be found in [1]–[4]

However the experimental measurement of permeability is time consuming and results can vary depending on the experimental method. Furthermore, direct measurement of unsaturated permeability is even more challenging given the fact that having control over all the contributing parameters is hard to achieve. Therefore, the unsaturated permeability is usually indirectly determined using inverse analysis of weight loss experiments [2], [5].

Considering the importance of permeability and experimental challenges to overcome, there have been various attempts to model permeability starting from classical models such as Kozeny's work [6] that relates the permeability to the porosity and later modified by Carman known as Kozeny–Carman equation [7]. The Katz-Thompson model [8] that was initially developed to predict the permeability of sedimentary rocks and relates the permeability to microstructure of the cementitious material using an analytical approach. And more recently with advancements in numerical approaches there has been several studies to estimate transport properties of cementitious materials. To mention a few, G. Ye et.al [9] presented a network model by means of extracting the pore space from simulated cement microstructure and embedding them into a network. They estimated the fluid flow by applying Hagen–Poiseuille law on the conduits and calculated the intrinsic permeability using Darcy's law. Their model only accounted for capillary porosity, which implies that there will be overestimation of the permeability value. Such an overestimation was also encountered by Li and Xu [10] who computed microstructure of various hardening cement pastes by means of the hydration kinetics model, HYMOSTRUC3D, which was then used to estimate intrinsic permeability using a finite element method. Song et.al [11] studied the microstructure of hydrated cement paste extracted from concrete using FIB/SEM (Focused Ion Beam/Scanning Electron Microscope) method, where a representative volume element (RVE) and its pore size distribution (PSD) were analyzed. Using a lattice Boltzmann method (LBM), they predicted intrinsic permeability of three samples. However, they underestimated the values by an order or magnitude, which was attributed to not capturing larger capillary pores and microcracks in the RVE. Yu et.al [12] proposed an interesting fractal based modelling framework, firstly to simulate the microstructure of cement paste and secondly to study the implication of this model on heat and mass transport properties of the material. The scope of their study is an RVE size of 200×200×200 µm with voxel size of 0.2 µm, which is verified against HYMOSTRUC with

reasonable agreement. In particular, intrinsic permeability was overestimated by orders of magnitude as not all sub-micron pores were not captured.

While the above work is confined to intrinsic permeability, Zalzale et.al[13] applied a 3D lattice Boltzmann technique to model permeability at different degrees of saturation. In addition to permeable micron-sized capillary pores, they managed to also include weakly-permeable nano-porous calcium silicate hydrate (C-S-H) pores in their model. The critical parameters, C-S-H density and capillary porosity, were taken from ^{1}H *(hydrogen)* nuclear magnetic resonance relaxation analysis. Their model however accounted only for variation of capillary PSD and applied pore blocking of these pores. Their pore blocking algorithm was based on the principle that the biggest pores gets blocked first regardless of their location. Kai Li et.al[14], [15] employed discrete element method (DEM) to generate and characterize microstructures and estimated the permeability using conventional moisture transfer equation. However, their microstructure only included the capillary pores and the gel pores were neglected. Their computational approach for unsaturated permeability is similar to Zalzale et.al[13], [16]. In a recent attempt to model relative permeability, Ecay et.al [17] used an analytical approach, which is essentially an extension of the model proposed by Khaddor [18] that describes the evolution of the intrinsic permeability of mortar undergoing micro-cracking. The model is based on a hierarchical assembly of capillaries with decreasing diameter, generated randomly. Estimated intrinsic as well as relative permeability are in close agreement with experiments and mostly falls within the same order of magnitude unlike other studies reported above, hence a promising approach given no model calibration and no computational burden.

Alternatively, a numerically efficient approach to simulate water transport in porous materials is the pore network model pioneered by Mason [19], [20], which is the primary modelling tool utilized in the study presented further in this paper. Finally, a comprehensive review of pore

network modelling can be found in[4] and a recent review on water permeability of unsaturated cementitious materials is available in [21].

All these previously proposed models either require some empirical or experimental parameters involved in the modelling or they do not take all the pore size range of the material into account. Therefore, this paper presents a numerical study on permeability based on a multiscale approach, which can drive the information from microstructure and integrate them into a representative numerical framework to model both intrinsic and unsaturated permeability. This numerical framework starts from fundamental information, which are chemical composition of the cement and reaction conditions such as age, curing, etc. Thus, no experimental calibration would be needed. The framework consists of different modelling tools comprising, microstructure modelling to model the microstructure and provide capillary PSD, particle packing to estimate gel PSD, and pore network modelling, which integrates the entire range of PSD and arrives at a statistically representative pore network, which is used as a basis to carry out moisture transport calculations. In order to evaluate the capability of the proposed pore network modelling framework, it is validated against an extensive set of existing experimental data that includes a wide range of cementitious materials [1], [3], [5], [22]–[27].

2 Multiscale pore network

The pore network is constructed using hierarchical homogenization of pore space (Figure 1) similar to that explained in Babaei et al.[28] with minor algorithmic changes explained in the following section. This has been done in order to improve the precision of the network construction for permeability, which is also more sensitive to spatial distribution and arrangement of pore classes.

Hardened cement paste (HCP) formed from the cement hydration reaction has a hierarchical multiscale structure. If the hardened cement paste is represented in two different scales of (i) C-S-H level and (ii) cement paste level, then porosity of each level can be distinguished as follows: (i) low (LD) and high density (HD) C-S-H being the porous phases in level-1 and capillary porosity in cement paste level-2 (Figure 1). Therefore, a representative pore space is constructed by combining these three network at different scales as illustrated in Figure 2.

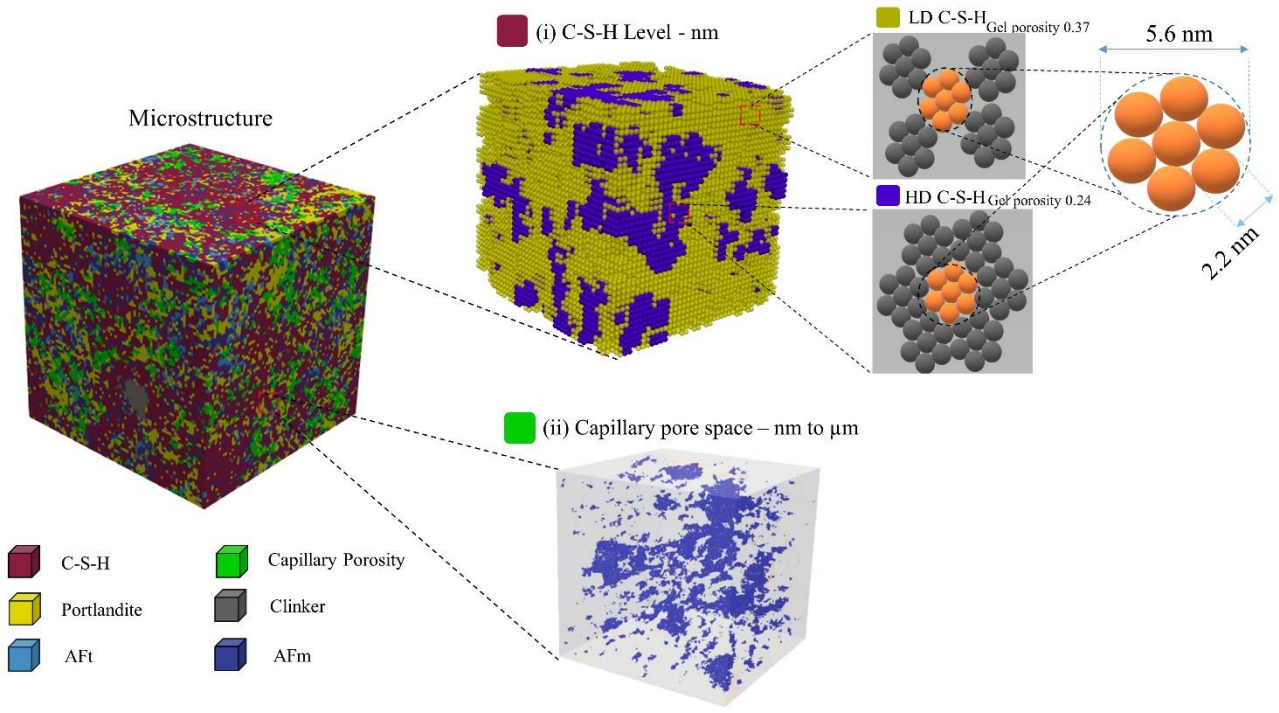

Figure 1. Illustration of the microstructure and the pore space within the proposed multiscale modeling hierarchical network

What varies depending on the final microstructure of hardened cement paste is the ratio of the volumetric fraction of these pore classes and their respective PSD. In level-1 the PSD of each individual phase including LD and HD C-S-H is constant, while their ratio (volume fraction) is the main parameter, which changes depending of reaction parameters such as water/cement ratio (w/c), age, curing method, etc. At level-2 both PSD and volume fraction of capillary porosity can change. As computation of hydration reactions using existing cement hydration kinetics models from nano scale to tens of micro meter is computationally expensive, the microstructure is modelled via a two-step process, first the microstructure and hydration reaction at level-2 are modeled by a cement hydration kinetics model VCCTL [29] that provides various parameters such as w/c, cement composition, curing and age. More details are available in [29]. Then the ratio of LD and HD at level-1 is calculated based on Jennings-Tennis hydration

model. With respect to PSD here the particle packing is used to calculate the PSD of LD and HD C-S-H based on [28], [30], while VCCTL is used to compute capillary porosity and its size distribution. VCCTL simulate hydration reaction in a 100×100×100 μm RVE. Once the pore size distribution and volume fraction of the capillary pores are known they will be embedded in a cubic network filled with gel pores obtained from the particle packing model. This resembles the same hierarchical composition of the microstructure with C-S-H gel as the matrix and capillary pores as voids. Note that it is assumed that there are no pores within other hydration products other than C-S-H gel.

In Babaei et al. [28], [31], the network was constructed to determine the saturation degree at different relative humidity (*RH*) and thus the volume fraction of each pore class would be directly transferred to the network meaning that if the pore space consists of 0.5 gel pores and 0.5 capillary pores in terms of volume fraction then the same ratio in terms of volume fraction would have to exist in the network as well. Therefore, the resulting network would be much bigger (in terms of number of pores). However, in this study, in order to transfer the data from microstructure to the pore network the volume fraction of each pore class is converted to their population number. For instance, a microstructure with capillary porosity of 0.25 and 0.6 C-S-H gel in microstructure level, is represented by 1.47 million of capillary pores and 1 million of gel pores assuming the gel porosity is 0.28 [32], [33]. Network generation is carried out in four steps:

(i) An initial cubic network with size of 100 μm and 1 million pores is created for homogenized network at C-S-H level.

(ii) Largest fraction at level-1 (i.e., LD or HD C-S-H) is chosen as the master phase and added to the network. Their population is calculated based on the LD/HD ratio at

level-1 and total number amounts to 1 million pores. i.e. $n_{master}\ C-S-H = Dominant\ C-S-H\ phase \times 10^6$.

(iii) Pores of secondary phase (phase with smaller fraction) at level-1 are added to the master network to form a homogenized network at level-1 holding HD and LD C-S-H gel pores.

(iv) The capillary pores are randomly distributed in the homogenized gel network to form a network, which includes all the three pore classes. The number of capillary pores are equal to $n_{capillary} = \left({capillary\ porosity}/{gel\ porosity}\right) \times 10^6$.

(v) Throats are added to connect pores and their size is calibrated as described in Babaei et al.[28], [30].

Once the pores are embedded, there are multiple possible ways to connect them, the coordination number in this study is assumed to be six as it ensures enough connectivity within different classes of pores and also does not over facilitate the flow in the network as cementitious materials are known to be weakly permeable [28], [30]. Regarding the size and length of this connecting throats the same values are applied as mentioned in Babaei et al.[28], [30]. It is also worth recalling that there is a missing gap between the two scales as the biggest gel pore is only 12 nm and smallest capillary pore possible with microstructural modelling is 1 μm. This information gap is however addressed using a numerical approximation as explained in section 2.3 in Babaei et al. [28].

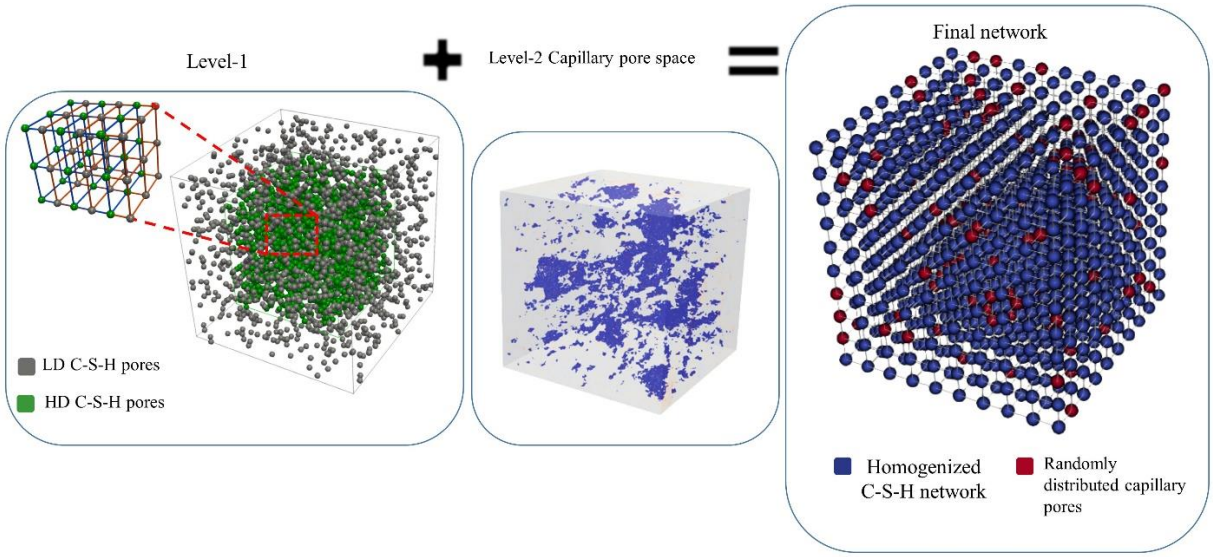

Figure 2. Pore space at two different levels and their homogenization

3 Permeability calculations

3.1 General principle

The general principle of computing permeability from the constructed pore network is to apply a water pressure gradient across any two opposite faces of the network and computing average water flux. Darcy's law can then be invoked to back calculate the permeability of the network as follows:

$$Q = K_l \frac{A}{\mu L} \Delta P \quad (1)$$

where Q is the flow rate (m^3/s), A is the network cross section area (m^2), L is length of the network (m), μ is the dynamic viscosity (Pa.s), ΔP is pressure difference across the two opposing sides (Pa), and K_l is permeability of the network (m^2).

This formulation is applicable for water filled conduits only, i.e. for saturated porous medium. In the following sections, algorithms to compute intrinsic and unsaturated permeability are detailed.

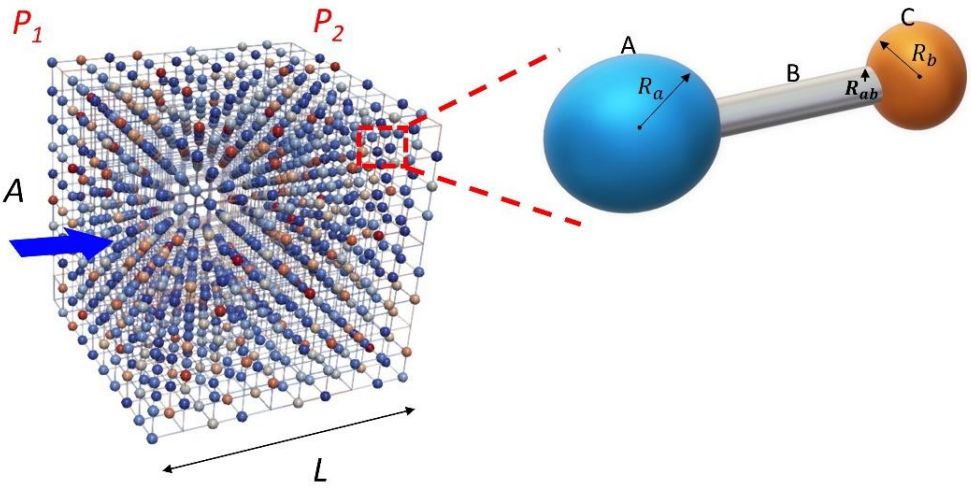

Figure 3. Measurement of intrinsic permeability by applying pressure gradient (P_1-P_2).

3.2 Intrinsic permeability

The intrinsic permeability is independent of measurement factors such as, measurement method, sample size, pressure gradient, etc., and depends solely on pore space structure of the cementitious material.

The method described below essentially provides an estimation of the intrinsic permeability, meaning that all the pores are contributing to the flow rate and are fully saturated. In order to compute the flow through the network an exact solution of Navier-Stokes equation, i.e. the Hagen-Poiseuille's law is applied for each conduit formed by two neighbouring pores and their

connecting throat. The flow rate, q_c, and hydraulic resistance, R, for each conduit is computed via [34], [35]:

$$q_c = R\,\Delta P \qquad (2)$$

$$R = \left[\frac{1}{R_{p1}} + \frac{1}{R_t} + \frac{1}{R_{p2}}\right]^{-1} \qquad (3)$$

where *p1*, *t* and *p2* refers to pore *1*, throat and pore *2*, respectively that forms one conduit system. Throats have a constant diameter and Hagen–Poiseuille's law is directly applicable for computing their hydraulic resistance, but since the pores in the generated network are assumed to be spheres, they have varying cross section, depending on the connecting throat diameter in the entire network. Therefore, to compute R of each conduit the approach proposed by Akbari et.al.[34] for slightly varying micro-channels is used as follows:

$$R = {}^{q}/_{\Delta P} = \left[16\pi^2\mu \int_{x_1}^{x_2} \frac{I_p^*}{A^2}\,dx\right]^{-1} \qquad (4)$$

where $I_p^* = {}^{I_p}/_{A^2}$ with $I_p = \int_A (y^2 + z^2)dA$ is called the specific polar moment of cross-sectional inertia. μ is the dynamic viscosity, A_1 and A_2 are the cross sectional area at x_1 and x_2 as in (Figure 4), and y and z are Cartesian co-ordinates.

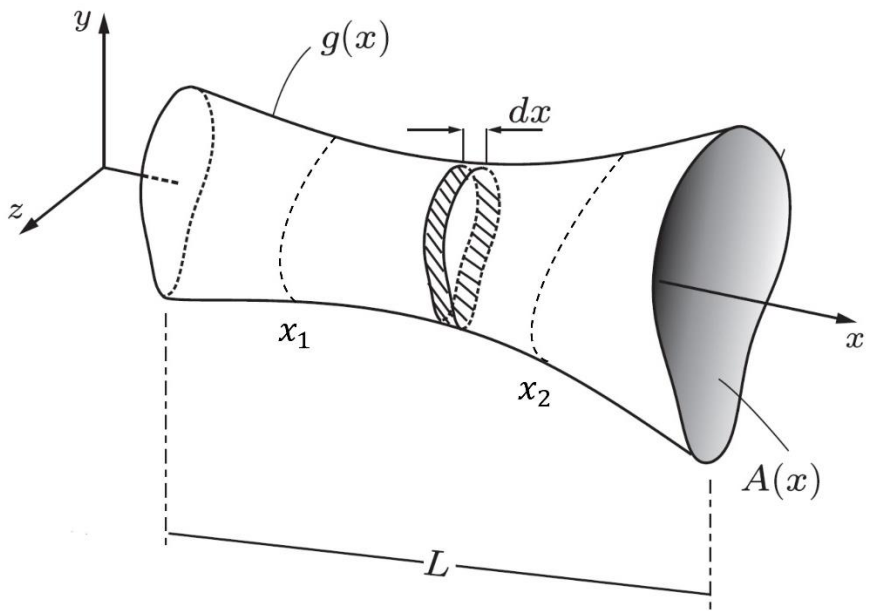

Figure 4. Geometry of a slightly varying micro-channel adapted from [34]

Once, the hydraulic resistances of all the conduits in the pore network are computed, an arbitrary positive pressure gradient is applied on any two opposite faces of the network (say in the *x* direction), with zero flux imposed on the remaining faces. The following mass conservation is solved for each pore as follows:

$$\sum_{j=1}^{n} R_{i,j}.(x_i - x_j) = 0 \qquad (5)$$

where *j* is the index of neighbouring pores, and it varies from 2 to 7 because the coordination number of each pore is considered as 6. $R_{i,j}$ is the hydraulic resistance between *i* and *j*, and *x* is the unknown quantity being solved for, which is the pressure field here. For instance for pore *i*=1 and its neighboring pores of *j*=(2,3,4,5,6,7), it results in:

$$-(R_{1,2} + R_{1,3} + R_{1,4} + R_{1,5} + R_{1,6} + R_{1,7}).x_1 + R_{1,2}.x_2 + R_{1,3}.x_3 + R_{1,4}.x_4 + R_{1,5}.x_5 + R_{1,6}.x_6 + R_{1,7}.x_7 = 0 \qquad (6)$$

For the entire pore network the mass conservation equations can be assembled to calculate the unknown pressure field, **x**:

$$\boldsymbol{x} = \boldsymbol{A}^{-1}\boldsymbol{b} \qquad (7)$$

where **A** is a matrix composed of coefficient of $\mathbf{x}_i$ in accordance with the Equation (6) for each pore in the network. The vector **b** contains components of the boundary condition, which is a constant arbitrary pressure applied on two sides of the network i.e., Dirichlet boundary condition. The flow field is computed based on the calculated pressure field as explained above. Finally, to determine the network's effective water permeability, the total flow rate is calculated at the boundary pores lying in a plane perpendicular to the flow direction. The water permeability is then obtained via Eq.(1) as explained earlier.

The calculations are repeated for the remaining pairs of opposite faces or sides to yield permeability in all mutually perpendicular directions. Finally, the average of the three permeability values are computed.

3.3 Unsaturated permeability

The calculated intrinsic permeability is not valid for partially saturated state in which some of the pores are empty and thus do not contribute to the water flow. In order to simulate *RH* of the partially saturated material, two independent algorithms are implemented and executed in parallel on the same network to resemble realistic partially saturated flow mechanism. The calculation methodology is the same as intrinsic permeability for network generation and calculation of hydraulic resistance. However, a preceding step involves running an invasion algorithm [36], which simulates drying process in response to the external boundary condition, which in this instance is the capillary pressure, P_c. Invasion algorithm essentially invades air phase into the network from all sides following the approach described in [28] or in other words

conduits get desaturated in accordance with the applied P_c on the boundaries. A specific capillary pressure in which a pore or throat can be invaded is computed using Young–Laplace equation as Eq.(7) in [28].

The relative permeability is then computed via a number of sequential iterations of invasion algorithm and permeability simulation as follows (Figure 5):

(i) The intrinsic permeability is calculated at P_c=0 Pa (or RH=1), i.e. for the fully saturated network. For this an arbitrary positive pressure gradient is applied across any two opposite sides as discussed in Section 3.2.

(ii) Invasion algorithm is applied on the network by incrementing P_c to desaturate the pores. The pores and throats, which are invaded (or desaturated) are assigned to be blocked from water flow. It is worth noting that in this study pore and throats can be only either open to water flow or blocked.

(iii) The permeability of the partially blocked network will be determined in accordance with step (i) above.

(iv) The above sequence is continued for different increments of P_c to cover the entire range of degree of saturation (or RH). It is obvious that when the degree of saturation of the network is close to zero, most of the network conduits are blocked.

In the example shown in Figure 5, four snapshots of desaturation of fully saturated structure is shown. In this illustration, the invasion algorithm is only applied on one side normal to the flow for clearer visualization. The desaturated pores seen in yellow colour are the ones that are blocked for water flow.

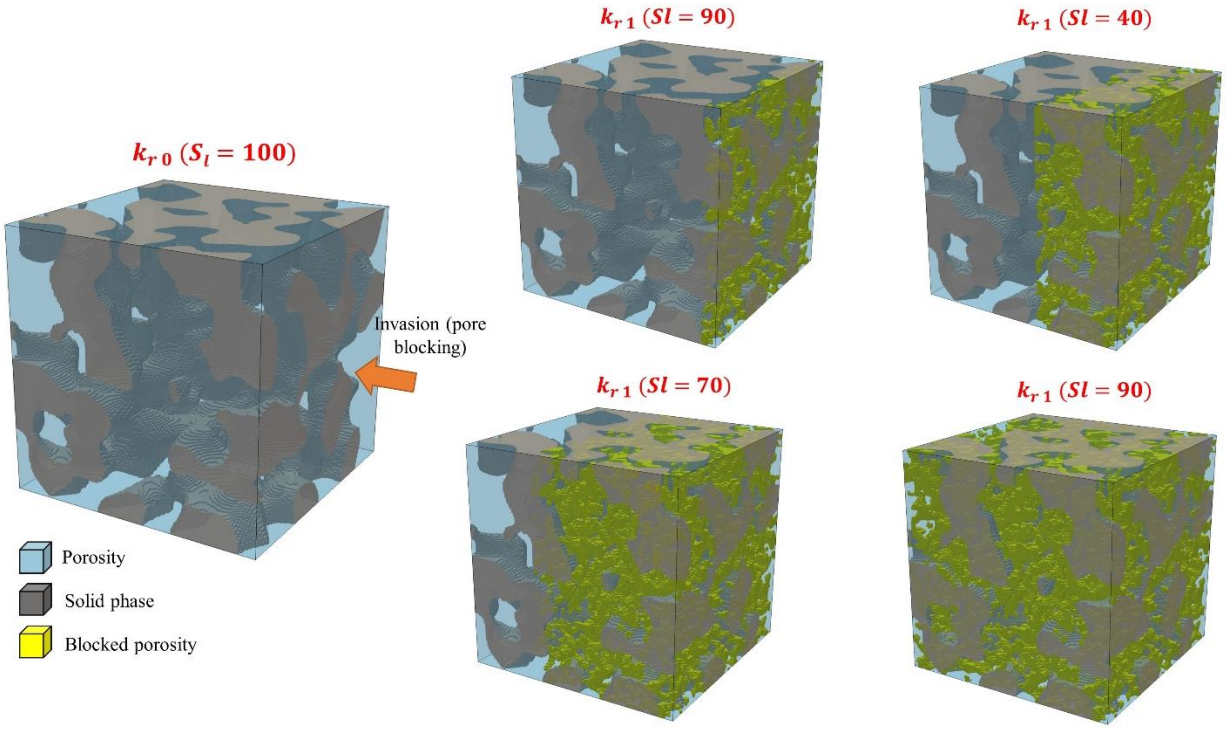

Figure 5. Sequential invasion of the network and calculating the relative permeability for each sequence (4 different degree of saturations).

4 Results and validation

The method proposed in this paper is validated against an extensive number of experiments available in literature. The validation is conducted in two parts: (i) intrinsic and (ii) unsaturated permeability. Table 1 shows the experimental details of each dataset. Note that the measured value for intrinsic permeability may differ depending on the experimental approach [2], [5], [37] and it can vary up to an order of magnitude and even higher[2], [5]. That is why an estimation within a range of order of magnitude is still seen as acceptable in this study. In addition to measurement uncertainties, there can be back calculation error effect involved in reported values, for example, when the permeability is back calculated using Van Genuchten [38]retention curve but the fitting is not perfect.

Table 1. Experimental data from literature [1]–[3], [5], [22]–[27]. *HCP: Hardened cement paste*

Material	Author	Measurement method	Material Type	W/C	Age (days)	Curing	Intrinsic permeability (m^2)
CP1	Baroghel-Bouny (1999)	Inverse analysis from mass loss	CEM I - HCP	0.34	365	Sealed then vacuum rewetted	10^{-21}
CP2	Ai et al (2001)	Thermo-permeametry	CEM I + 6% silica fume - HCP	0.4	548	Sealed and moist cured for 24 h then cured underwater	8.65×10^{-22}
CP3	Ye (2005)	Pressure cell	CEM I - HCP	0.4	28	Sealed then vacuum rewetted	9×10^{-22}
CP4				0.5			1.33×10^{-19}
CP5				0.6			1.82×10^{-18}
CP6	Grasley (2007)	Dynamic pressurization (DP)	CEM I - HCP	0.5	80	Limewater	3×10^{-21}
CP7				0.6	32		6.5×10^{-21}
CP8	Phung (2013)	Constant flow	CEM I - HCP	0.4	28	Limewater	8×10^{-21}
CP9				0.5			3×10^{-20}
CP10				0.6			7×10^{-20}
CP11	Kumar (2014)	MIP	CEM I - HCP	0.45	28	sealed	4×10^{-21}
CP12				0.5			1×10^{-20}

CP13				0.64			2×10^{-19}
CP14	Zamani (2014)	Inverse analysis	CEM I - HCP	0.4	28	Under water	4×10^{-21}
CP15	Egan (2017)	Inverse analysis	CEM I - HCP	0.45	56	Limewater	3×10^{-21}
CP16				0.55			6×10^{-21}
CP17				0.65			2×10^{-20}
CP18	Zhang (2018)	Beam Bending - Sorptivity	CEM I - HCP	0.5	365	Limewater	Avg.= 1.2×10^{-19}

313

4.1 Intrinsic permeability

The estimation of permeability involves carrying out microstructural modelling (hydration calculations) using the cement composition data reported by various researchers (OPC, CEM I here, only CP2 includes 6% silica fume). The results from the microstructural model is presented in Table 2, based on which pore network is constructed for each material composition, which is subsequently taken forward to estimate permeability. Note that to simulate permeability, 18 pore networks have been constructed corresponding to the 18 data sets available in Table 2. Table 2 also reports the intrinsic permeability measured in all three directions for each individual material, denoted as k_{0xx}, k_{0yy} *and* k_{0zz}. The results show that the k_0 values in different directions do not vary more than 3% indicating the representativeness of the network generated. A comparison of results from the proposed method against experimental observations are presented in Figure 6.

Table 2. The microstructure information of the studied materials.

Material	C3S (wt%)	C2S (wt%)	C3A (wt%)	C4AF (wt%)	W/C (wt%)	C-S-H (vol%)	LD C-S-H (vol%)	HD C-S-H (vol%)	Capillary Porosity (vol%)	Total Porosity (vol%)	Estimated Permeability (m^2) – k_0	Average Estimated Permeability (m^2) – k_0
CP1	57.28	23.98	3.03	7.59	0.34	0.50	0.18	0.32	0.12	0.24	$k_{0xx}=8.59\times10^{-22}$ $k_{0yy}=8.38\times10^{-22}$ $k_{0zz}=8.55\times10^{-22}$	8.51×10^{-22}
CP2	67.1	17.5	7.7	7.6	0.4	0.47	0.22	0.25	0.13	0.25	$k_{0xx}=1.29\times10^{-21}$ $k_{0yy}=1.25\times10^{-21}$ $k_{0zz}=1.26\times10^{-21}$	1.27×10^{-21}
CP3	63	13	8	9	0.4	0.47	0.22	0.25	0.14	0.25	$k_{0xx}=4.08\times10^{-21}$ $k_{0yy}=3.97\times10^{-21}$ $k_{0zz}=3.95\times10^{-21}$	4.00×10^{-21}
CP4					0.5	0.46	0.33	0.13	0.19	0.29	$k_{0xx}=2.17\times10^{-20}$ $k_{0yy}=2.22\times10^{-20}$ $k_{0zz}=2.23\times10^{-20}$	2.21×10^{-20}
CP5					0.6	0.46	0.37	0.09	0.23	0.33	$k_{0xx}=4.65\times10^{-19}$ $k_{0yy}=4.69\times10^{-19}$ $k_{0zz}=4.81\times10^{-19}$	4.72×10^{-19}
CP6	48.3	21.5	7.6	9.1	0.5	0.47	0.33	0.14	0.19	0.30	$k_{0xx}=1.91\times10^{-21}$ $k_{0yy}=1.93\times10^{-21}$ $k_{0zz}=1.97\times10^{-21}$	1.94×10^{-21}
CP7					0.6	0.46	0.36	0.10	0.22	0.32	$k_{0xx}=7.89\times10^{-20}$ $k_{0yy}=7.93\times10^{-20}$	7.86×10^{-20}

											$k_{0zz}=7.75\times10^{-20}$	
CP8	62.5	18	9	10	0.4	0.44	0.21	0.23	0.14	0.25	$k_{0xx}=4.41\times10^{-21}$ $k_{0yy}=4.53\times10^{-21}$ $k_{0zz}=4.39\times10^{-21}$	4.45×10^{-21}
CP9					0.5	0.44	0.32	0.12	0.19	0.30	$k_{0xx}=2.80\times10^{-20}$ $k_{0yy}=2.71\times10^{-20}$ $k_{0zz}=2.73\times10^{-20}$	2.75×10^{-20}
CP10					0.6	0.45	0.40	0.05	0.24	0.34	$k_{0xx}=1.18\times10^{-19}$ $k_{0yy}=1.15\times10^{-19}$ $k_{0zz}=1.17\times10^{-19}$	1.17×10^{-19}
CP11	59.2	16.7	9	10.3	0.45	0.49	0.29	0.20	0.18	0.29	$k_{0xx}=1.11\times10^{-20}$ $k_{0yy}=1.12\times10^{-20}$ $k_{0zz}=1.15\times10^{-20}$	1.13×10^{-20}
CP12					0.5	0.49	0.35	0.14	0.20	0.32	$k_{0xx}=2.58\times10^{-20}$ $k_{0yy}=2.49\times10^{-20}$ $k_{0zz}=2.51\times10^{-20}$	2.53×10^{-20}
CP13					0.64	0.46	0.40	0.06	0.27	0.37	$k_{0xx}=6.29\times10^{-19}$ $k_{0yy}=6.45\times10^{-19}$ $k_{0zz}=6.42\times10^{-19}$	6.39×10^{-19}
CP14	66.9	20	3.5	4.4	0.4	0.52	0.25	0.27	0.14	0.27	$k_{0xx}=2.29\times10^{-21}$ $k_{0yy}=2.38\times10^{-21}$ $k_{0zz}=2.30\times10^{-21}$	2.33×10^{-21}
CP15	56.5	18	6.3	11.4	0.45	0.46	0.28	0.18	0.17	0.28	$k_{0xx}=1.08\times10^{-20}$ $k_{0yy}=1.14\times10^{-20}$ $k_{0zz}=1.10\times10^{-20}$	1.11×10^{-20}

CP16					0.55	0.45	0.38	0.07	0.22	0.32	$k_{0xx}=5.31\times10^{-20}$ $k_{0yy}=5.45\times10^{-20}$ $k_{0zz}=5.42\times10^{-20}$	5.40×10^{-20}
CP17					0.65	0.44	0.38	0.06	0.26	0.36	$k_{0xx}=4.25\times10^{-19}$ $k_{0yy}=4.29\times10^{-19}$ $k_{0zz}=4.21\times10^{-19}$	4.25×10^{-19}
CP18	53.6	17.5	7.5	8.8	0.5	0.46	0.33	0.13	0.19	0.29	$k_{0xx}=2.74\times10^{-20}$ $k_{0yy}=2.67\times10^{-20}$ $k_{0zz}=2.73\times10^{-20}$	2.72×10^{-20}

327

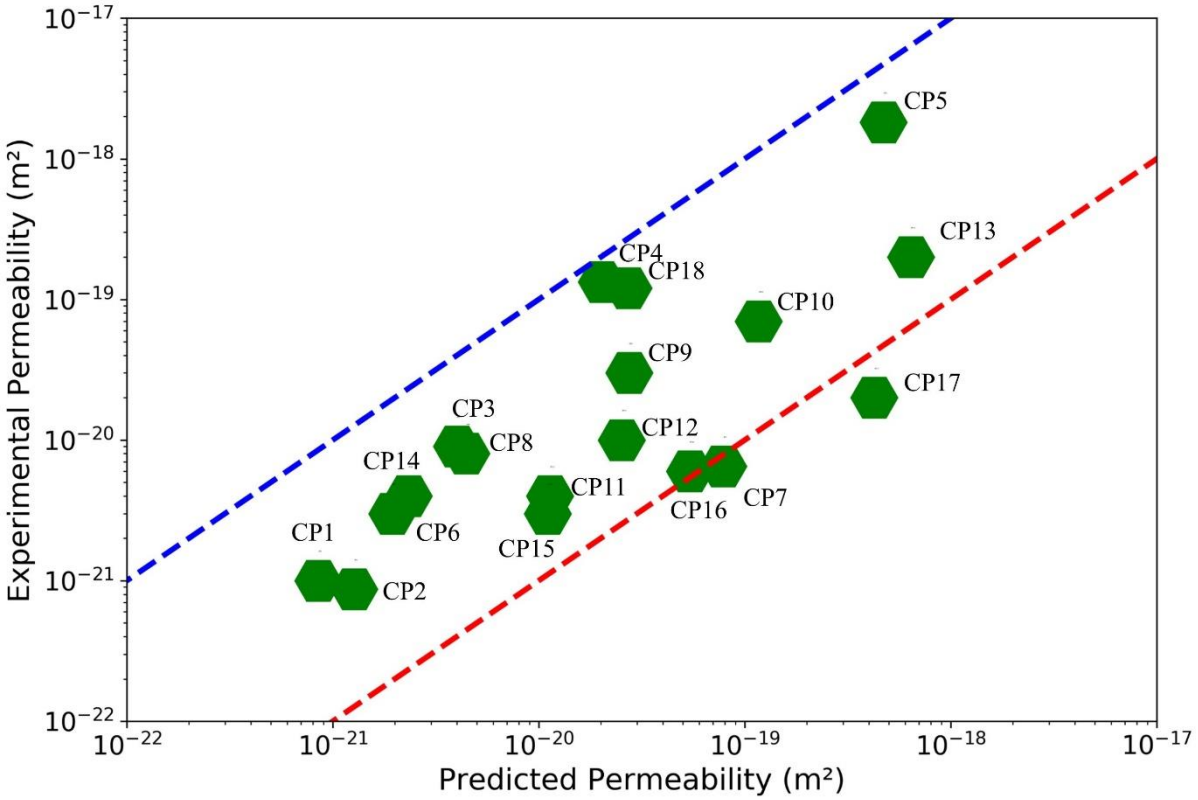

Figure 6. Estimated values using pore network modelling vs. experimental observations (dash lines order of magnitude lines).

Overall, the model results show a very good correspondence with the experimental observations. In fact, the results fall well within the same order of magnitude for 17 out of 18 studied cases. This confirms that the proposed model can successfully and systematically transfer information from microstructure into a pore network, which is representative of permeability of HCP.

The predicted value for CP17 is the only case where the model fails to estimate within the same order of magnitude as the experimentally observed value. However, in this case, the permeability is indirectly measured; firstly fitting a Van Genuchten [38] curve on experimental retention curve and then back calculating the mass loss using the fitted Van Genuchten curve. This method however is sensitive to fitting parameters of the retention curve and thus can be

affected by the accuracy of fitting. Moreover, different types of measurements can lead to different results and this is mainly due to experimental uncertainties. For instance, CP13 and CP17 have a relatively similar composition but the measured permeability for CP13 is exactly one order of magnitude less than that of CP17, while ratio of their permeability estimated by the proposed model is 3. The same argument holds for CP16, whose permeability value lies just at the border of the order of magnitude line.

The experimentally measured value for CP7, which is an OPC with W/C of 0.6 is 6.5×10^{-21} m^2 that is at least an order of magnitude lower than similar compositions with the same W/C ratio (CP5, CP10) and using different experimental methods. As already mentioned, the measurement method can also affect the measured value and this seems to be the case here. Furthermore, the estimated values using pore network seems to be mostly close to the values measured by constant flow and indirect measurements (inverse analysis).

In terms of improved accuracy the accuracy of proposed methodology compared to previous studies that targeted modelling the same variables, using comparable tools [9], [10], [14], [21] is considerably more e.g., in [10] the permeability of CP3-CP5 were (over)estimated in range of 10^{-16} -10^{-14} as opposed to 10^{-21} -10^{-19} in this study.

From the microstructural modelling results presented in Table 2, it is seen that the permeability can be correlated with the ratio of HD and LD C-S-H at C-S-H level and the capillary porosity at microstructure level. A parametric analysis (Figure 7) shows that for the study cases the permeability is directly proportional to the capillary porosity (*Figure 7* (a)) and inversely proportional to the HD C-S-H gel porosity (*Figure 7* (b)), which is the lowest permeable phase of C-S-H. In terms of comparative parameters, consistent trends for $V_{LD\ C\text{-}S\text{-}H}/V_{HD\ C\text{-}S\text{-}H}$ (*Figure 7* (c)) and $V_{capillary}/V_{total\ porosity}$ ratios (*Figure 7* (d)) are also observed (V_i denotes volume fraction

of phase i). The R^2 values sort the correlation of the parameters and permeability in the order of capillary porosity with R^2=0.82, capillary/total porosity with R^2=0.79 and $V_{LD\ C\text{-}S\text{-}H}$ /$V_{HD\ C\text{-}S\text{-}H}$ with R^2=0.64. The parametric analysis also shows that both capillary porosity (which is present in level-2) and C-S-H gel content (level-1) are important and contributing to the transport in hardened cement paste. While what has been concluded here is valid for mature pastes i.e., older than 28 days, it has been reported that at early age (1-10 days) the capillary porosity plays a more important role in permeability compared to the gel porosity. This is to be expected at early age due to higher connectivity of capillary pore space and lower degrees of hydration, which translates to coarser pore space [9], [24], [39], [40].

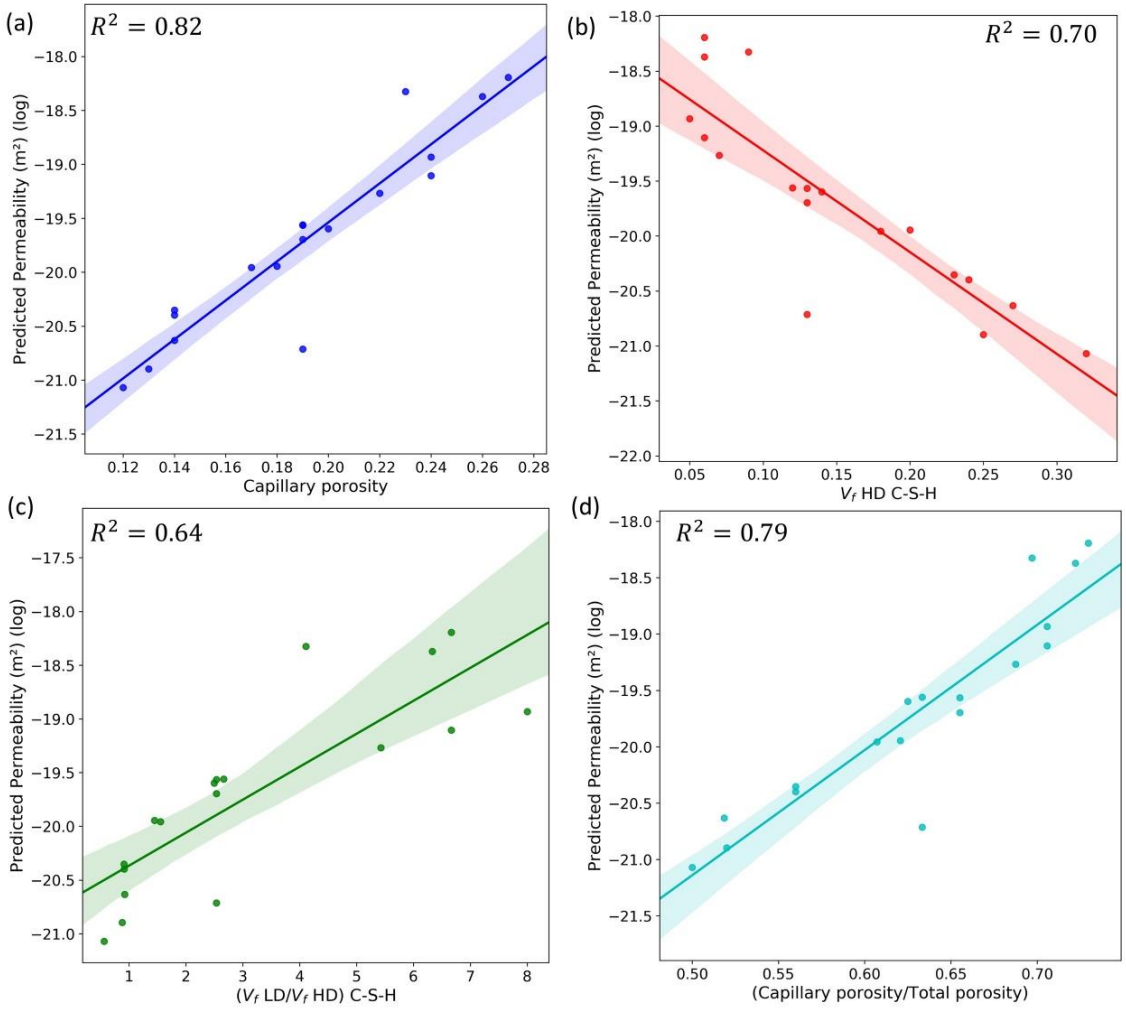

374

375 *Figure 7. Parametric analysis of intrinsic permeability for the studied materials.*

4.2 Unsaturated permeability

For the material CP1 and CP18 the unsaturated permeability values are available based on the inverse analysis, which will be used for comparisons. Additionally, comparisons will be made against the unsaturated permeability obtained from a calibrated water retention curve using the well-known Van Genuchten [38] model.

The Van Genuchten model for retention curve and unsaturated permeability are defined as follows:

$$S_l = \left[\left(\left(\frac{p_c}{a_{mu}}\right)^{\frac{b_{mu}}{b_{mu}-1}} + 1\right)^{-\frac{1}{b_{mu}}}\right] \quad (8)$$

where a_{mu} and b_{mu} are fitting parameters, which require fitting for each set of water sorption experiments available for the materials CP1 and CP18.

The unsaturated permeability is defined as:

$$k_l = k_0 k_{rl}(S_l) \quad (9)$$

where k_0 is the intrinsic permeability for CP1 and CP18 (Table 2) and $k_{rl}(S_l)$ is the relative permeability defined as :

$$k_{rl} = {S_l}^{0.5}\left[\left(1 - \left(1 - {S_l}^{b_{mu}}\right)^{\frac{1}{b_{mu}}}\right)^2\right] \quad (10)$$

Figure 8 shows a comparison of the results of the pore network model and the Van Genuchten model and the experimental data from the mass loss experiments for the materials CP1 and CP18. For both materials, the pore network model is more accurate than the Van Genuchten model. This proves not only that the network is representative for intrinsic permeability

simulation, but also for unsaturated scenarios where the constructed network can provide better results compared to the classical models. The advantage of the proposed framework lies in the fact that it contains more information and relevance from the material, while such relevance and link is missing in case of empirical models. Note that the experimental trend for CP1 is unreliable because it shows that the unsaturated permeability is higher at lower degrees of saturation. This is likely to be caused by experimental uncertainties [2], [5], [25].

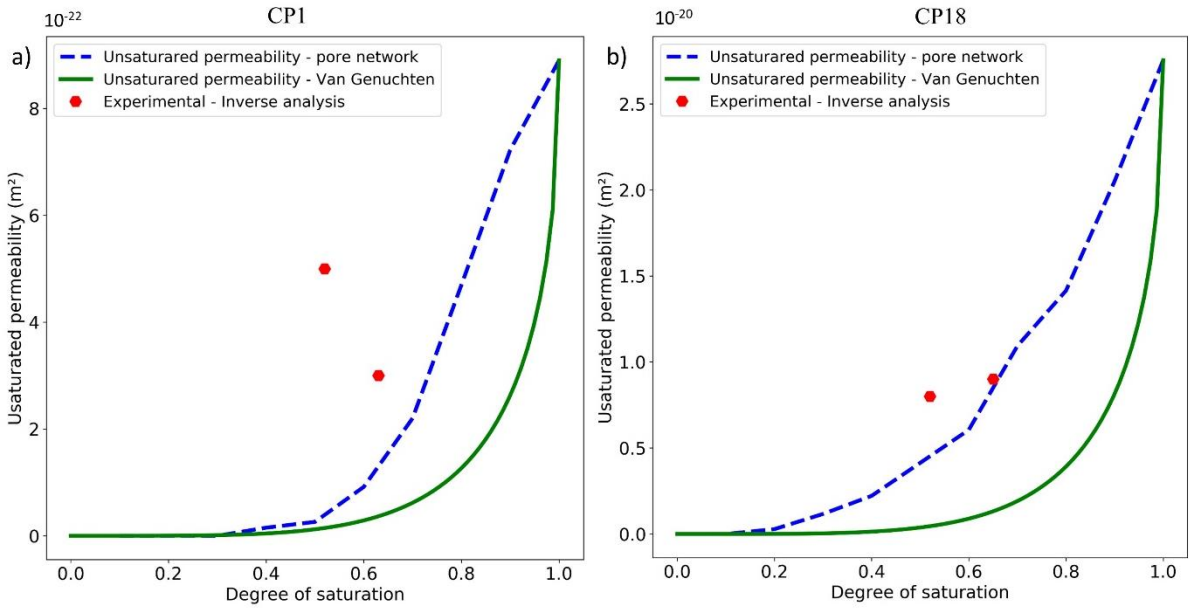

Figure 8. Unsaturated permeability estimated using pore network VS. experimental measurements

It is also worth noting that the unsaturated permeability estimated by pore network as well as the experimentally measured values roughly remain in the same order of magnitude of the intrinsic permeability up to *RH*=0.5. At this *RH*, pores with size of approximately 12 nm are desaturated. Pores smaller than 12 nm are mostly small capillary pores and gel pores. This indicates that gel pores are also contributing to the flow, even though because of their size they are weakly permeable, and their contribution is definitely not negligible as was suggested in [13], [16]. One additional conclusion to be drawn is that up to 50% *RH* the water permeability would still be in the range of intrinsic permeability indicating that moisture flow in the liquid

phase is the major mechanism in this range as argued previously by multiple authors, to mention a few [2], [5], [25], [41]. In other words, no two phase flow model is necessary to model moisture flow in unsaturated cement paste up to this *RH* level.

5 Conclusions

This study presents a new and fundamentally predictive methodology for computation of intrinsic and unsaturated permeability of OPC-based cementitious materials. The proposed methodology utilizes a multiscale numerical framework starting from cement composition and its microstructure to constructing a hierarchical pore network and computation of the permeability. Moreover, a novel multi-algorithmic approach is developed to compute unsaturated permeability at different degrees of saturation. This framework adopts different modeling tools including (i) particle packing for modelling the pore size distribution of the C-S-H gel pores, (ii) microstructural modelling to model hydration reaction kinetics, and (iii) pore network modelling. The microstructure is modelled using VCCTL software and pore network modelling used here is a customized version of OpenPNM [42] developed in python using mainly NumPy [43] and SciPy[44], [45] libraries. A quasi-static analysis of the network using Hagen–Poiseuille coupled with Young-Laplace equation (in a form of invasion algorithm [36]) is then invoked in pore bodies and throats to estimate saturated and unsaturated permeability, the Young-Laplace equation because the invasion algorithm resembles the drying by invading and blocking pores and throats.

The proposed approach is validated against eighteen different experiments available in the literature and obtained results are remarkably promising, indicating the flexibility and reliability of the framework. Additionally, a parametric analysis on dependency of intrinsic water permeability on microstructural variables such as capillary porosity, volume fraction of HD C-S-H etc., showed that the permeability can be correlated to the variables from both the level-1 (C-S-H gel level) and level-2 (capillary porosity). Finally, it was also observed that the proposed model can provide a more accurate results compared to Van Genuchten for unsaturated water permeability.

In terms of disadvantage of the proposed framework, its reliance on microstructural modelling and all the initial inputs that are derived herewith could have a negative impact on the final estimation if the microstructure is not accurate in reporting the phase fractions. Secondly, the applicability of the framework on blended cement systems is not investigated because of the lack of established microstructural modelling for these materials. However, CP2 in the studied materials includes 6% silica fume and estimated permeability is also fairly accurate. But applicability on systems with high percentage of additives such as limestone calcined cement [46], [47] remains uncertain. Finally, the proposed model is intended to operate at microstructural level with RVE size of few 100s of micrometers with no consideration of microcracks. Whereas in reality permeability experiments are carried out at centimeter scale and hence any effect of microcracks on permeability cannot be captured by this version of the model. However, this limitation can be easily overcome by adding synthetic microcracks into the RVE.

Acknowledgements

The first author gratefully acknowledges PhD sponsorship offered by SCK CEN. The findings and conclusions in this paper are those of the authors and do not represent the official position of SCK CEN. The authors are also grateful for insightful discussions with Dr. Tri Quoc Phung, and for the constructive criticisms of anonymous reviewers of this paper.

REFERENCES

[1] Q. T. Phung, N. Maes, G. De Schutter, D. Jacques, and G. Ye, "Determination of water permeability of cementitious materials using a controlled constant flow method," *Constr. Build. Mater.*, vol. 47, pp. 1488–1496, 2013, doi: https://doi.org/10.1016/j.conbuildmat.2013.06.074.

[2] Z. Zhang, M. Thiery, and V. Baroghel-Bouny, "Investigation of moisture transport properties of cementitious materials," *Cem. Concr. Res.*, vol. 89, pp. 257–268, 2016, doi: https://doi.org/10.1016/j.cemconres.2016.08.013.

[3] A. Kumar, S. Ketel, K. Vance, T. Oey, N. Neithalath, and G. Sant, "Water Vapor Sorption in Cementitious Materials—Measurement, Modeling and Interpretation," *Transp. Porous Media*, vol. 103, no. 1, pp. 69–98, 2014, doi: 10.1007/s11242-014-0288-5.

[4] Q. Xiong, T. G. Baychev, and A. P. Jivkov, "Review of pore network modelling of porous media: Experimental characterisations, network constructions and applications to reactive transport," *J. Contam. Hydrol.*, vol. 192, pp. 101–117, 2016, doi: https://doi.org/10.1016/j.jconhyd.2016.07.002.

[5] Z. Zhang and G. Scherer, "Determination of water permeability for a moisture transport model with minimized batch effect," *Constr. Build. Mater.*, vol. 191, pp. 193–205, 2018, doi: https://doi.org/10.1016/j.conbuildmat.2018.09.194.

[6] M. Kozeny, "Uber kapillare Leitung des Wassers im Boden," *Sitzber. Akad. Wiss. Wein, Math-naturw*, vol. 136, p. Abt. II a, P. 277, 1927.

[7] P. C. Carman, “Fluid flow through granular beds,” *Chem. Eng. Res. Des.*, vol. 75, pp. S32–S48, 1997, doi: https://doi.org/10.1016/S0263-8762(97)80003-2.

[8] A. J. Katz and A. H. Thompson, “Quantitative prediction of permeability in porous rock,” *Phys. Rev. B*, vol. 34, no. 11, pp. 8179–8181, Dec. 1986, doi: 10.1103/PhysRevB.34.8179.

[9] G. Ye, P. Lura, and K. van Breugel, “Modelling of water permeability in cementitious materials,” *Mater. Struct.*, vol. 39, no. 9, pp. 877–885, 2006, doi: 10.1617/s11527-006-9138-4.

[10] X. Li and Y. Xu, “Microstructure-Based Modeling for Water Permeability of Hydrating Cement Paste,” *J. Adv. Concr. Technol.*, vol. 17, no. 7, pp. 405–418, 2019, doi: 10.3151/jact.17.405.

[11] Y. Song, G. Dai, L. Zhao, Z. Bian, P. Li, and L. Song, “Permeability prediction of hydrated cement paste based on its 3D image analysis,” *Constr. Build. Mater.*, vol. 247, p. 118527, 2020, doi: https://doi.org/10.1016/j.conbuildmat.2020.118527.

[12] P. Yu, Y. H. Duan, E. Chen, S. W. Tang, and X. R. Wang, “Microstructure-based fractal models for heat and mass transport properties of cement paste,” *Int. J. Heat Mass Transf.*, vol. 126, pp. 432–447, 2018, doi: https://doi.org/10.1016/j.ijheatmasstransfer.2018.05.150.

[13] M. Zalzale, P. J. McDonald, and K. L. Scrivener, “A 3D lattice Boltzmann effective media study: understanding the role of C-S-H and water saturation on the permeability of cement paste,” *Model. Simul. Mater. Sci. Eng.*, vol. 21, no. 8, p. 85016, 2013, doi:

10.1088/0965-0393/21/8/085016.

[14] K. Li, P. Stroeven, and N. L. B. Le, “METHODOLOGY FOR POROSIMETRY IN VIRTUAL CEMENTITIOUS COMPOSITES TO ECONOMICALLY AND RELIABLY ESTIMATE PERMEABILITY,” *Image Anal. & Stereol. Vol 34, No 2 (2015)DO - 10.5566/ias.1271* , May 2015, [Online]. Available: https://www.ias-iss.org/ojs/IAS/article/view/1271.

[15] K. Li, “Numerical Determination of Permeability in Unsaturated Cementitious Materials,” Delft University of Technology, 2017.

[16] M. Zalzale and P. J. McDonald, “Lattice Boltzmann simulations of the permeability and capillary adsorption of cement model microstructures,” *Cem. Concr. Res.*, vol. 42, no. 12, pp. 1601–1610, 2012, doi: https://doi.org/10.1016/j.cemconres.2012.09.003.

[17] L. Ecay, D. Grégoire, and G. Pijaudier-Cabot, “On the prediction of permeability and relative permeability from pore size distributions,” *Cem. Concr. Res.*, vol. 133, p. 106074, 2020, doi: https://doi.org/10.1016/j.cemconres.2020.106074.

[18] K. Fadi, G. David, and P.-C. Gilles, “A Hierarchical Model for the Computation of Permeation Properties of Porous Materials and Their Enhancement due to Microcracks,” *J. Eng. Mech.*, vol. 144, no. 2, p. 4017160, Feb. 2018, doi: 10.1061/(ASCE)EM.1943-7889.0001392.

[19] G. Mason, “The effect of pore space connectivity on the hysteresis of capillary condensation in adsorption—desorption isotherms,” *J. Colloid Interface Sci.*, vol. 88, no. 1, pp. 36–46, 1982, doi: https://doi.org/10.1016/0021-9797(82)90153-9.

[20] G. Mason and D. H. Everett, “A model of adsorption-desorption hysteresis in which hysteresis is primarily developed by the interconnections in a network of pores,” *Proc. R. Soc. London. A. Math. Phys. Sci.*, vol. 390, no. 1798, pp. 47–72, Nov. 1983, doi: 10.1098/rspa.1983.0122.

[21] K. Li, L. Xu, P. Stroeven, and C. Shi, “Water permeability of unsaturated cementitious materials: A review,” *Constr. Build. Mater.*, vol. 302, p. 124168, 2021, doi: https://doi.org/10.1016/j.conbuildmat.2021.124168.

[22] Z. C. Grasley, G. W. Scherer, D. A. Lange, and J. J. Valenza, “Dynamic pressurization method for measuring permeability and modulus: II. cementitious materials,” *Mater. Struct.*, vol. 40, no. 7, pp. 711–721, 2007, doi: 10.1617/s11527-006-9184-y.

[23] H. Ai, J. F. Young, and G. W. Scherer, “Thermal Expansion Kinetics: Method to Measure Permeability of Cementitious Materials: II, Application to Hardened Cement Pastes,” *J. Am. Ceram. Soc.*, vol. 84, no. 2, pp. 385–391, Feb. 2001, doi: https://doi.org/10.1111/j.1151-2916.2001.tb00666.x.

[24] G. Ye, “Percolation of capillary pores in hardening cement pastes,” *Cem. Concr. Res.*, vol. 35, no. 1, pp. 167–176, 2005, doi: https://doi.org/10.1016/j.cemconres.2004.07.033.

[25] V. Baroghel-Bouny, M. Mainguy, T. Lassabatere, and O. Coussy, “Characterization and identification of equilibrium and transfer moisture properties for ordinary and high-performance cementitious materials,” *Cem. Concr. Res.*, vol. 29, no. 8, pp. 1225–1238, 1999, doi: https://doi.org/10.1016/S0008-8846(99)00102-7.

[26] S. Zamani, R. M. Kowalczyk, and P. J. McDonald, “The relative humidity dependence of the permeability of cement paste measured using GARField NMR profiling,” *Cem. Concr. Res.*, vol. 57, pp. 88–94, 2014, doi: https://doi.org/10.1016/j.cemconres.2013.12.010.

[27] G. Egan, A. Kumar, N. Neithalath, and G. Sant, “Re-examining the influence of the inclusion characteristics on the drying shrinkage of cementitious composites,” *Constr. Build. Mater.*, vol. 146, pp. 713–722, 2017, doi: https://doi.org/10.1016/j.conbuildmat.2017.04.048.

[28] S. Babaei, S. C. Seetharam, U. Muehlich, A. Dizier, G. Steenackers, and B. Craeye, “A multiscale framework to estimate water sorption isotherms for OPC-based materials,” *Cem. Concr. Compos.*, vol. 105, p. 103415, 2020, doi: https://doi.org/10.1016/j.cemconcomp.2019.103415.

[29] J. Bullard, “Virtual Cement and Concrete Testing Laboratory: Version 9.5 User Guide.” Special Publication (NIST SP), National Institute of Standards and Technology, Gaithersburg, MD, 2014.

[30] S. Babaei, *A multiscale approach to model thermo-hydro-mechanical behaviour of nonreinforced concrete* . Antwerp: University of Antwerp, Faculty of Applied Engineering, 2021.

[31] S. Babaei, S. C. Seetharam, A. Dizier, G. Steenackers, and B. Craeye, “An analytical framework for estimating drying shrinkage strain of OPC based hardened cement paste,” *Cem. Concr. Compos.*, vol. 115, p. 103833, 2021, doi: https://doi.org/10.1016/j.cemconcomp.2020.103833.

[32] D. P. Bentz, “Three-Dimensional Computer Simulation of Portland Cement Hydration and Microstructure Development,” *J. Am. Ceram. Soc.*, vol. 80, no. 1, pp. 3–21, Jan. 1997, doi: https://doi.org/10.1111/j.1151-2916.1997.tb02785.x.

[33] T. C. POWERS, “Structure and Physical Properties of Hardened Portland Cement Paste,” *J. Am. Ceram. Soc.*, vol. 41, no. 1, pp. 1–6, Jan. 1958, doi: https://doi.org/10.1111/j.1151-2916.1958.tb13494.x.

[34] M. Akbari, D. Sinton, and M. Bahrami, “Viscous flow in variable cross-section microchannels of arbitrary shapes,” *Int. J. Heat Mass Transf.*, vol. 54, no. 17, pp. 3970–3978, 2011, doi: https://doi.org/10.1016/j.ijheatmasstransfer.2011.04.028.

[35] M. Islahuddin and H. Janssen, “Hygric property estimation of porous building materials with multiscale pore structures,” *Energy Procedia*, vol. 132, pp. 273–278, 2017, doi: https://doi.org/10.1016/j.egypro.2017.09.722.

[36] D. Wilkinson and J. F. Willemsen, “Invasion percolation: a new form of percolation theory,” *J. Phys. A. Math. Gen.*, vol. 16, no. 14, pp. 3365–3376, 1983, doi: 10.1088/0305-4470/16/14/028.

[37] S. Goto and D. M. Roy, “The effect of w/c ratio and curing temperature on the permeability of hardened cement paste,” *Cem. Concr. Res.*, vol. 11, no. 4, pp. 575–579, 1981, doi: https://doi.org/10.1016/0008-8846(81)90087-9.

[38] M. T. van Genuchten, “A Closed-form Equation for Predicting the Hydraulic Conductivity of Unsaturated Soils,” *Soil Sci. Soc. Am. J.*, vol. 44, no. 5, pp. 892–898, Sep. 1980, doi: https://doi.org/10.2136/sssaj1980.03615995004400050002x.

[39] M. Zhang, “Pore-scale modelling of relative permeability of cementitious materials using X-ray computed microtomography images,” *Cem. Concr. Res.*, vol. 95, pp. 18–29, 2017, doi: https://doi.org/10.1016/j.cemconres.2017.02.005.

[40] M. Bogdan, “Morphological multisscale modeling of cementitious materials -- Application to effective diffusive properties prediction,” École normale supérieure de Cachan - ENS Cachan, 2015.

[41] V. Baroghel-Bouny, “Water vapour sorption experiments on hardened cementitious materials: Part I: Essential tool for analysis of hygral behaviour and its relation to pore structure,” *Cem. Concr. Res.*, vol. 37, no. 3, pp. 414–437, 2007, doi: https://doi.org/10.1016/j.cemconres.2006.11.019.

[42] J. Gostick *et al.*, “OpenPNM: A Pore Network Modeling Package,” *Comput. Sci. Eng.*, vol. 18, no. 4, pp. 60–74, 2016, doi: 10.1109/MCSE.2016.49.

[43] C. R. Harris *et al.*, “Array programming with NumPy,” *Nature*, vol. 585, no. 7825, pp. 357–362, 2020, doi: 10.1038/s41586-020-2649-2.

[44] P. Virtanen *et al.*, “SciPy 1.0: fundamental algorithms for scientific computing in Python,” *Nat. Methods*, vol. 17, no. 3, pp. 261–272, Mar. 2020, doi: 10.1038/s41592-019-0686-2.

[45] S. van der Walt *et al.*, “scikit-image: image processing in Python,” *PeerJ*, vol. 2, p. e453, 2014, doi: 10.7717/peerj.453.

[46] K. L. Scrivener, V. M. John, and E. M. Gartner, “Eco-efficient cements: Potential economically viable solutions for a low-CO2 cement-based materials industry,” *Cem.*

Concr. Res., vol. 114, pp. 2–26, 2018, doi: https://doi.org/10.1016/j.cemconres.2018.03.015.

[47] W. Wilson, L. Sorelli, and A. Tagnit-Hamou, "Unveiling micro-chemo-mechanical properties of C–(A)–S–H and other phases in blended-cement pastes," *Cem. Concr. Res.*, vol. 107, pp. 317–336, 2018, doi: https://doi.org/10.1016/j.cemconres.2018.02.010.

Permeability of Cementitious Materials using a Multiscale Pore Network Model

Saeid Babaei* [(1)a,b,c], Suresh C. Seetharam [(2)b], Arnaud Dizier[(3)d], Gunther Steenackers[(4)c,e] and Bart Craeye[(5)c,f]

[a] SVK N.V., Aerschotstraat 114 B-9100 Sint-Niklaas, Belgium.

[b] Engineered and Geosystems Analysis Unit, Institute for Environment, Health, and Safety, Belgian Nuclear Research Centre (SCK•CEN), Boeretang 200, B-2400 Mol, Belgium.

[c] Faculty of Applied Engineering, University of Antwerp, EMIB Research Group, Groenenborgerlaan 171 - 2020 Antwerpen , Belgium.

[d] EIG, EURIDICE, Belgian Nuclear Research Centre (SCK•CEN), Boeretang 200, B-2400 Mol, Belgium.

[e] Faculty of Applied Engineering, University of Antwerp | Op3Mech Research Group Groenenborgerlaan 171 - 2020 Antwerpen.

[f] Odisse University College, Industrial Services & Technologies, DUBIT Research Unit, Belgium.

(1) Tel: +32 474740440, saeid.babaei@svk.be; saeid.babaei@uantwerpen.be

(2) Tel: +32 14 333208, suresh.seetharam@sckcen.be

(3) Tel: +32 14 332998, arnaud.dizier@euridice.be

(4) Tel: +32 00 000000, gunther.steenackers@uantwerpen.be

(5) Tel: +32 00 000000, bart.craeye@uantwerpen.be

Abstract

This paper presents a new multiscale pore network modelling framework for predicting saturated and unsaturated permeability of OPC-based cementitious materials using a novel algorithmic implementation. The framework fundamentally relies on the data on cement composition and current understanding of cement hydration kinetics and microstructural features. Central to the modelling framework is the ability to numerically estimate pore size distribution (PSD) from existing models and the ability to obtain snapshots of unsaturated microstructure for various degrees of saturation. The framework is an amalgamation of three important existing models: (i) particle packing model for predicting nanoscale PSD, (ii) cement hydration kinetics to estimate microscale PSD, and (iii) a pore network model to estimate the permeability. The proposed pore network modelling is validated against an extensive set of experimental data that includes a very wide range of materials. The predicted intrinsic permeability falls well within the accepted experimental range. Though fewer experimental data are available to compare, the predicted unsaturated permeability shows highly promising results.

1 Introduction

Cementitious materials are ubiquitously used in urbanization. Besides their classical use in construction, these materials are also envisioned for use both as encapsulation of radioactive waste and as engineered barriers for disposal of radioactive waste. One of the major governing parameters for performance and safety assessment of cementitious materials is their permeability because this has a direct link with the transport mechanisms of aggressive substances responsible for degradation of the cementitious matrix. In addition, it is a measure of how the cementitious material can withstand drying due to environmental loading (e.g. atmospheric or heat induced), which can have a decisive impact on shrinkage induced cracks. The intrinsic water permeability, also called specific permeability or absolute permeability, is the measured permeability for a fully saturated state. The unsaturated water permeability or relative permeability is the measured permeability at lower degrees of saturation. However, measuring permeability is not straightforward and there are two main approaches to measure it in laboratory, direct and indirect measurements. While the former is done usually by means of applying a certain pressure gradient or flow rate on a cylindrical sample and quantifying the permeability using Darcy's law, the latter approach involves either the application of a transient pressure pulse technique or the application of poromechanical techniques or inverse analysis of moisture loss experiments. A review of these experimental methods can be found in [1]–[4]

However the experimental measurement of permeability is time consuming and results can vary depending on the experimental method. Furthermore, direct measurement of unsaturated permeability is even more challenging given the fact that having control over all the contributing parameters is hard to achieve. Therefore, the unsaturated permeability is usually indirectly determined using inverse analysis of weight loss experiments [2], [5].

Considering the importance of permeability and experimental challenges to overcome, there have been various attempts to model permeability starting from classical models such as Kozeny's work [6] that relates the permeability to the porosity and later modified by Carman known as Kozeny–Carman equation [7]. The Katz-Thompson model [8] that was initially developed to predict the permeability of sedimentary rocks and relates the permeability to microstructure of the cementitious material using an analytical approach. And more recently with advancements in numerical approaches there has been several studies to estimate transport properties of cementitious materials. To mention a few, G. Ye et.al [9] presented a network model by means of extracting the pore space from simulated cement microstructure and embedding them into a network. They estimated the fluid flow by applying Hagen–Poiseuille law on the conduits and calculated the intrinsic permeability using Darcy's law. Their model only accounted for capillary porosity, which implies that there will be overestimation of the permeability value. Such an overestimation was also encountered by Li and Xu [10] who computed microstructure of various hardening cement pastes by means of the hydration kinetics model, HYMOSTRUC3D, which was then used to estimate intrinsic permeability using a finite element method. Song et.al [11] studied the microstructure of hydrated cement paste extracted from concrete using FIB/SEM (Focused Ion Beam/Scanning Electron Microscope) method, where a representative volume element (RVE) and its pore size distribution (PSD) were analyzed. Using a lattice Boltzmann method (LBM), they predicted intrinsic permeability of three samples. However, they underestimated the values by an order or magnitude, which was attributed to not capturing larger capillary pores and microcracks in the RVE. Yu et.al [12] proposed an interesting fractal based modelling framework, firstly to simulate the microstructure of cement paste and secondly to study the implication of this model on heat and mass transport properties of the material. The scope of their study is an RVE size of 200×200×200 µm with voxel size of 0.2 µm, which is verified against HYMOSTRUC with

reasonable agreement. In particular, intrinsic permeability was overestimated by orders of magnitude as not all sub-micron pores were not captured.

While the above work is confined to intrinsic permeability, Zalzale et.al[13] applied a 3D lattice Boltzmann technique to model permeability at different degrees of saturation. In addition to permeable micron-sized capillary pores, they managed to also include weakly-permeable nano-porous calcium silicate hydrate (C-S-H) pores in their model. The critical parameters, C-S-H density and capillary porosity, were taken from ^{1}H *(hydrogen)* nuclear magnetic resonance relaxation analysis. Their model however accounted only for variation of capillary PSD and applied pore blocking of these pores. Their pore blocking algorithm was based on the principle that the biggest pores gets blocked first regardless of their location. Kai Li et.al[14], [15] employed discrete element method (DEM) to generate and characterize microstructures and estimated the permeability using conventional moisture transfer equation. However, their microstructure only included the capillary pores and the gel pores were neglected. Their computational approach for unsaturated permeability is similar to Zalzale et.al[13], [16]. In a recent attempt to model relative permeability, Ecay et.al [17] used an analytical approach, which is essentially an extension of the model proposed by Khaddor [18] that describes the evolution of the intrinsic permeability of mortar undergoing micro-cracking. The model is based on a hierarchical assembly of capillaries with decreasing diameter, generated randomly. Estimated intrinsic as well as relative permeability are in close agreement with experiments and mostly falls within the same order of magnitude unlike other studies reported above, hence a promising approach given no model calibration and no computational burden.

Alternatively, a numerically efficient approach to simulate water transport in porous materials is the pore network model pioneered by Mason [19], [20], which is the primary modelling tool utilized in the study presented further in this paper. Finally, a comprehensive review of pore

network modelling can be found in[4] and a recent review on water permeability of unsaturated cementitious materials is available in [21].

All these previously proposed models either require some empirical or experimental parameters involved in the modelling or they do not take all the pore size range of the material into account. Therefore, this paper presents a numerical study on permeability based on a multiscale approach, which can drive the information from microstructure and integrate them into a representative numerical framework to model both intrinsic and unsaturated permeability. This numerical framework starts from fundamental information, which are chemical composition of the cement and reaction conditions such as age, curing, etc. Thus, no experimental calibration would be needed. The framework consists of different modelling tools comprising, microstructure modelling to model the microstructure and provide capillary PSD, particle packing to estimate gel PSD, and pore network modelling, which integrates the entire range of PSD and arrives at a statistically representative pore network, which is used as a basis to carry out moisture transport calculations. In order to evaluate the capability of the proposed pore network modelling framework, it is validated against an extensive set of existing experimental data that includes a wide range of cementitious materials [1], [3], [5], [22]–[27].

2 Multiscale pore network

The pore network is constructed using hierarchical homogenization of pore space (Figure 1) similar to that explained in Babaei et al.[28] with minor algorithmic changes explained in the following section. This has been done in order to improve the precision of the network construction for permeability, which is also more sensitive to spatial distribution and arrangement of pore classes.

Hardened cement paste (HCP) formed from the cement hydration reaction has a hierarchical multiscale structure. If the hardened cement paste is represented in two different scales of (i) C-S-H level and (ii) cement paste level, then porosity of each level can be distinguished as follows: (i) low (LD) and high density (HD) C-S-H being the porous phases in level-1 and capillary porosity in cement paste level-2 (Figure 1). Therefore, a representative pore space is constructed by combining these three network at different scales as illustrated in Figure 2.

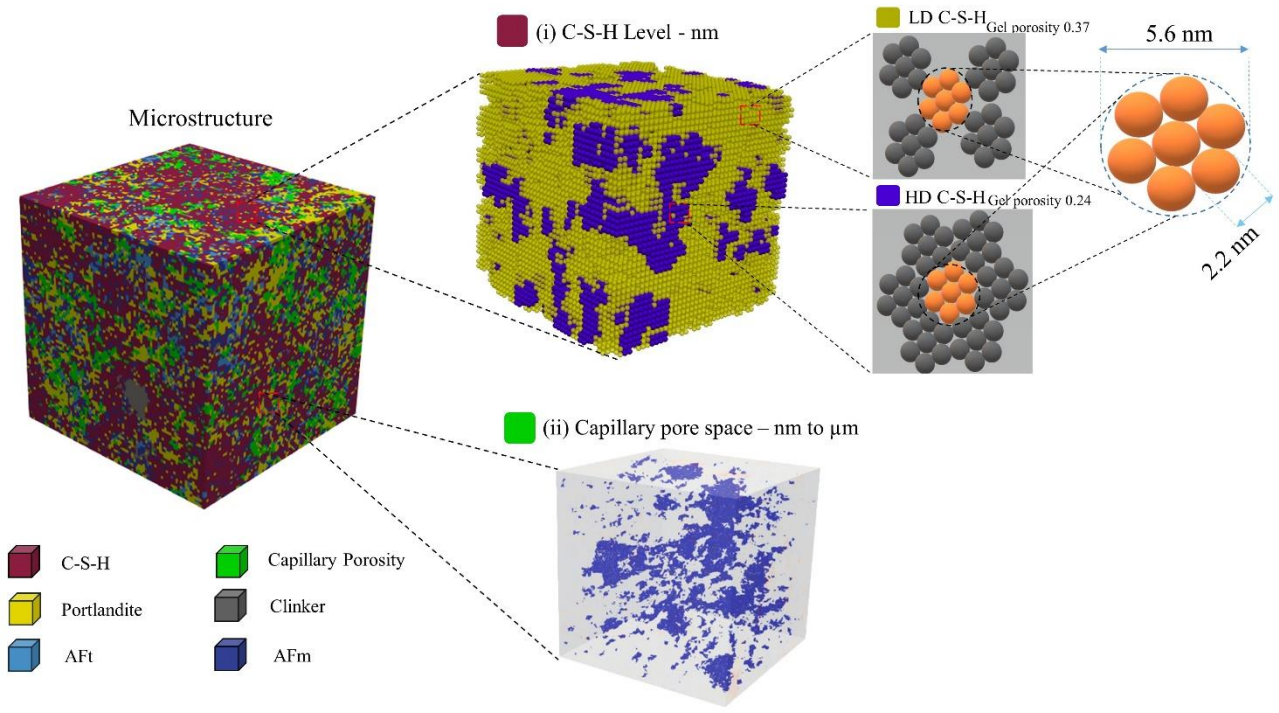

Figure 1. Illustration of the microstructure and the pore space within the proposed multiscale modeling hierarchical network

What varies depending on the final microstructure of hardened cement paste is the ratio of the volumetric fraction of these pore classes and their respective PSD. In level-1 the PSD of each individual phase including LD and HD C-S-H is constant, while their ratio (volume fraction) is the main parameter, which changes depending of reaction parameters such as water/cement ratio (w/c), age, curing method, etc. At level-2 both PSD and volume fraction of capillary porosity can change. As computation of hydration reactions using existing cement hydration kinetics models from nano scale to tens of micro meter is computationally expensive, the microstructure is modelled via a two-step process, first the microstructure and hydration reaction at level-2 are modeled by a cement hydration kinetics model VCCTL [29] that provides various parameters such as w/c, cement composition, curing and age. More details are available in [29]. Then the ratio of LD and HD at level-1 is calculated based on Jennings-Tennis hydration

model. With respect to PSD here the particle packing is used to calculate the PSD of LD and HD C-S-H based on [28], [30], while VCCTL is used to compute capillary porosity and its size distribution. VCCTL simulate hydration reaction in a 100×100×100 μm RVE. Once the pore size distribution and volume fraction of the capillary pores are known they will be embedded in a cubic network filled with gel pores obtained from the particle packing model. This resembles the same hierarchical composition of the microstructure with C-S-H gel as the matrix and capillary pores as voids. Note that it is assumed that there are no pores within other hydration products other than C-S-H gel.

In Babaei et al. [28], [31], the network was constructed to determine the saturation degree at different relative humidity (*RH*) and thus the volume fraction of each pore class would be directly transferred to the network meaning that if the pore space consists of 0.5 gel pores and 0.5 capillary pores in terms of volume fraction then the same ratio in terms of volume fraction would have to exist in the network as well. Therefore, the resulting network would be much bigger (in terms of number of pores). However, in this study, in order to transfer the data from microstructure to the pore network the volume fraction of each pore class is converted to their population number. For instance, a microstructure with capillary porosity of 0.25 and 0.6 C-S-H gel in microstructure level, is represented by 1.47 million of capillary pores and 1 million of gel pores assuming the gel porosity is 0.28 [32], [33]. Network generation is carried out in four steps:

(i) An initial cubic network with size of 100 μm and 1 million pores is created for homogenized network at C-S-H level.

(ii) Largest fraction at level-1 (i.e., LD or HD C-S-H) is chosen as the master phase and added to the network. Their population is calculated based on the LD/HD ratio at

level-1 and total number amounts to 1 million pores. i.e. $n_{master}\ C-S-H = Dominant\ C-S-H\ phase \times 10^6$.

(iii) Pores of secondary phase (phase with smaller fraction) at level-1 are added to the master network to form a homogenized network at level-1 holding HD and LD C-S-H gel pores.

(iv) The capillary pores are randomly distributed in the homogenized gel network to form a network, which includes all the three pore classes. The number of capillary pores are equal to $n_{capillary} = \left({capillary\ porosity}/{gel\ porosity}\right) \times 10^6$.

(v) Throats are added to connect pores and their size is calibrated as described in Babaei et al.[28], [30].

Once the pores are embedded, there are multiple possible ways to connect them, the coordination number in this study is assumed to be six as it ensures enough connectivity within different classes of pores and also does not over facilitate the flow in the network as cementitious materials are known to be weakly permeable [28], [30]. Regarding the size and length of this connecting throats the same values are applied as mentioned in Babaei et al.[28], [30]. It is also worth recalling that there is a missing gap between the two scales as the biggest gel pore is only 12 nm and smallest capillary pore possible with microstructural modelling is 1 μm. This information gap is however addressed using a numerical approximation as explained in section 2.3 in Babaei et al. [28].

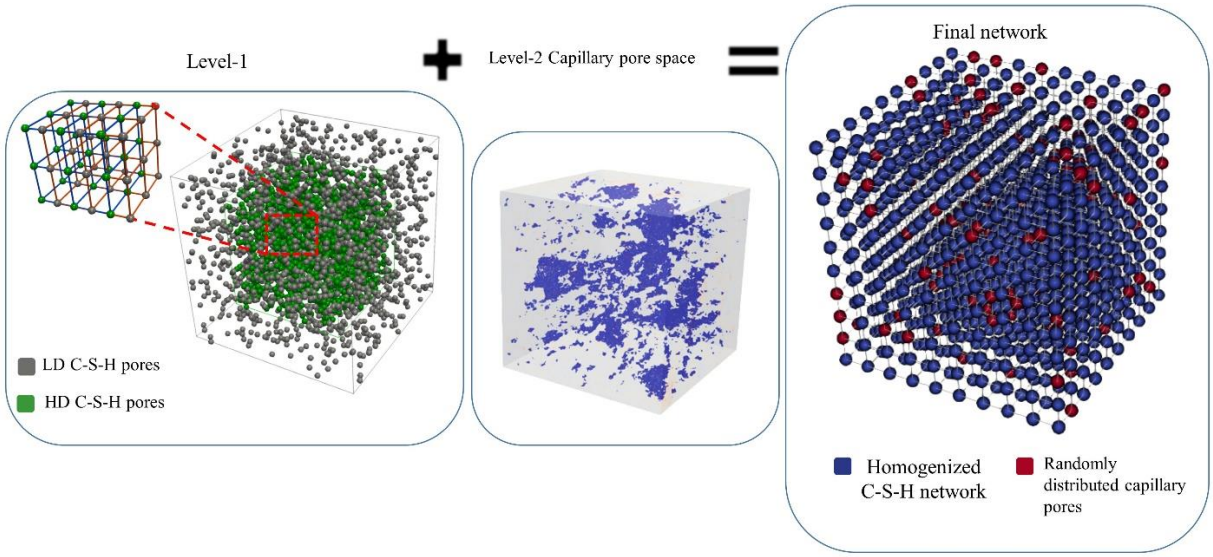

Figure 2. Pore space at two different levels and their homogenization

3 Permeability calculations

3.1 General principle

The general principle of computing permeability from the constructed pore network is to apply a water pressure gradient across any two opposite faces of the network and computing average water flux. Darcy's law can then be invoked to back calculate the permeability of the network as follows:

$$Q = K_l \frac{A}{\mu L} \Delta P \quad (1)$$

where Q is the flow rate (m^3/s), A is the network cross section area (m^2), L is length of the network (m), μ is the dynamic viscosity (Pa.s), ΔP is pressure difference across the two opposing sides (Pa), and K_l is permeability of the network (m^2).

This formulation is applicable for water filled conduits only, i.e. for saturated porous medium. In the following sections, algorithms to compute intrinsic and unsaturated permeability are detailed.

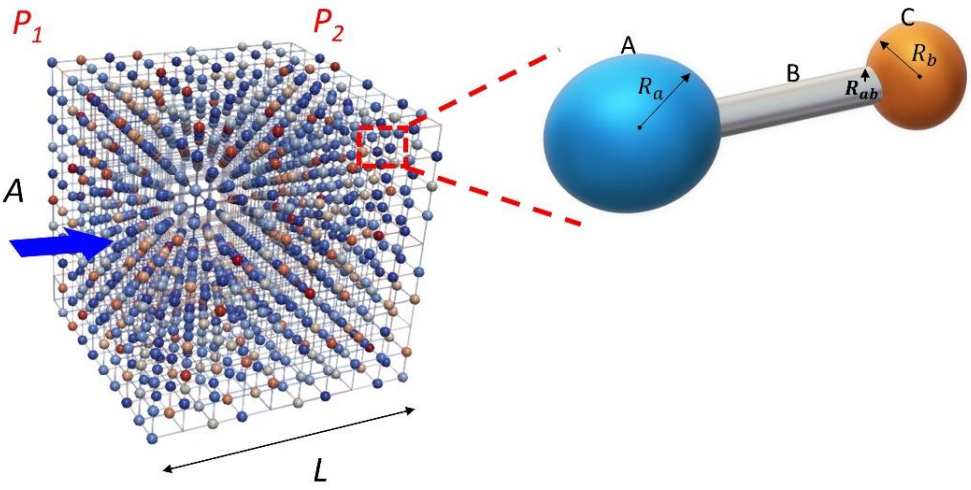

Figure 3. Measurement of intrinsic permeability by applying pressure gradient (P_1-P_2).

3.2 Intrinsic permeability

The intrinsic permeability is independent of measurement factors such as, measurement method, sample size, pressure gradient, etc., and depends solely on pore space structure of the cementitious material.

The method described below essentially provides an estimation of the intrinsic permeability, meaning that all the pores are contributing to the flow rate and are fully saturated. In order to compute the flow through the network an exact solution of Navier-Stokes equation, i.e. the Hagen-Poiseuille's law is applied for each conduit formed by two neighbouring pores and their

connecting throat. The flow rate, q_c, and hydraulic resistance, R, for each conduit is computed via [34], [35]:

$$q_c = R\,\Delta P \qquad (2)$$

$$R = \left[\frac{1}{R_{p1}} + \frac{1}{R_t} + \frac{1}{R_{p2}}\right]^{-1} \qquad (3)$$

where *p1*, *t* and *p2* refers to pore *1*, throat and pore *2*, respectively that forms one conduit system. Throats have a constant diameter and Hagen–Poiseuille's law is directly applicable for computing their hydraulic resistance, but since the pores in the generated network are assumed to be spheres, they have varying cross section, depending on the connecting throat diameter in the entire network. Therefore, to compute R of each conduit the approach proposed by Akbari et.al.[34] for slightly varying micro-channels is used as follows:

$$R = {}^{q}/_{\Delta P} = \left[16\pi^2\mu \int_{x_1}^{x_2} \frac{I_p^*}{A^2}\,dx\right]^{-1} \qquad (4)$$

where $I_p^* = {}^{I_p}/_{A^2}$ with $I_p = \int_A (y^2 + z^2)dA$ is called the specific polar moment of cross-sectional inertia. μ is the dynamic viscosity, A_1 and A_2 are the cross sectional area at x_1 and x_2 as in (Figure 4), and y and z are Cartesian co-ordinates.

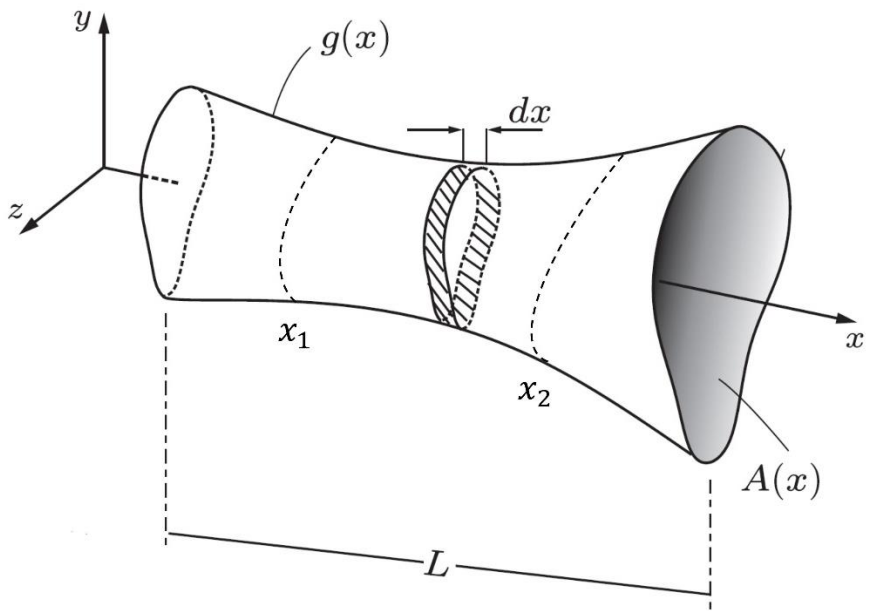

Figure 4. Geometry of a slightly varying micro-channel adapted from [34]

Once, the hydraulic resistances of all the conduits in the pore network are computed, an arbitrary positive pressure gradient is applied on any two opposite faces of the network (say in the *x* direction), with zero flux imposed on the remaining faces. The following mass conservation is solved for each pore as follows:

$$\sum_{j=1}^{n} R_{i,j}.(x_i - x_j) = 0 \qquad (5)$$

where *j* is the index of neighbouring pores, and it varies from 2 to 7 because the coordination number of each pore is considered as 6. $R_{i,j}$ is the hydraulic resistance between *i* and *j*, and *x* is the unknown quantity being solved for, which is the pressure field here. For instance for pore *i*=1 and its neighboring pores of *j*=(2,3,4,5,6,7), it results in:

$$-(R_{1,2} + R_{1,3} + R_{1,4} + R_{1,5} + R_{1,6} + R_{1,7}).x_1 + R_{1,2}.x_2 + R_{1,3}.x_3 + R_{1,4}.x_4 + R_{1,5}.x_5 + R_{1,6}.x_6 + R_{1,7}.x_7 = 0 \qquad (6)$$

For the entire pore network the mass conservation equations can be assembled to calculate the unknown pressure field, **x**:

$$\boldsymbol{x} = \boldsymbol{A}^{-1}\boldsymbol{b} \qquad (7)$$

where **A** is a matrix composed of coefficient of $\mathbf{x}_i$ in accordance with the Equation (6) for each pore in the network. The vector **b** contains components of the boundary condition, which is a constant arbitrary pressure applied on two sides of the network i.e., Dirichlet boundary condition. The flow field is computed based on the calculated pressure field as explained above. Finally, to determine the network's effective water permeability, the total flow rate is calculated at the boundary pores lying in a plane perpendicular to the flow direction. The water permeability is then obtained via Eq.(1) as explained earlier.

The calculations are repeated for the remaining pairs of opposite faces or sides to yield permeability in all mutually perpendicular directions. Finally, the average of the three permeability values are computed.

3.3 Unsaturated permeability

The calculated intrinsic permeability is not valid for partially saturated state in which some of the pores are empty and thus do not contribute to the water flow. In order to simulate *RH* of the partially saturated material, two independent algorithms are implemented and executed in parallel on the same network to resemble realistic partially saturated flow mechanism. The calculation methodology is the same as intrinsic permeability for network generation and calculation of hydraulic resistance. However, a preceding step involves running an invasion algorithm [36], which simulates drying process in response to the external boundary condition, which in this instance is the capillary pressure, P_c. Invasion algorithm essentially invades air phase into the network from all sides following the approach described in [28] or in other words

conduits get desaturated in accordance with the applied P_c on the boundaries. A specific capillary pressure in which a pore or throat can be invaded is computed using Young–Laplace equation as Eq.(7) in [28].

The relative permeability is then computed via a number of sequential iterations of invasion algorithm and permeability simulation as follows (Figure 5):

(i) The intrinsic permeability is calculated at P_c=0 Pa (or RH=1), i.e. for the fully saturated network. For this an arbitrary positive pressure gradient is applied across any two opposite sides as discussed in Section 3.2.

(ii) Invasion algorithm is applied on the network by incrementing P_c to desaturate the pores. The pores and throats, which are invaded (or desaturated) are assigned to be blocked from water flow. It is worth noting that in this study pore and throats can be only either open to water flow or blocked.

(iii) The permeability of the partially blocked network will be determined in accordance with step (i) above.

(iv) The above sequence is continued for different increments of P_c to cover the entire range of degree of saturation (or RH). It is obvious that when the degree of saturation of the network is close to zero, most of the network conduits are blocked.

In the example shown in Figure 5, four snapshots of desaturation of fully saturated structure is shown. In this illustration, the invasion algorithm is only applied on one side normal to the flow for clearer visualization. The desaturated pores seen in yellow colour are the ones that are blocked for water flow.

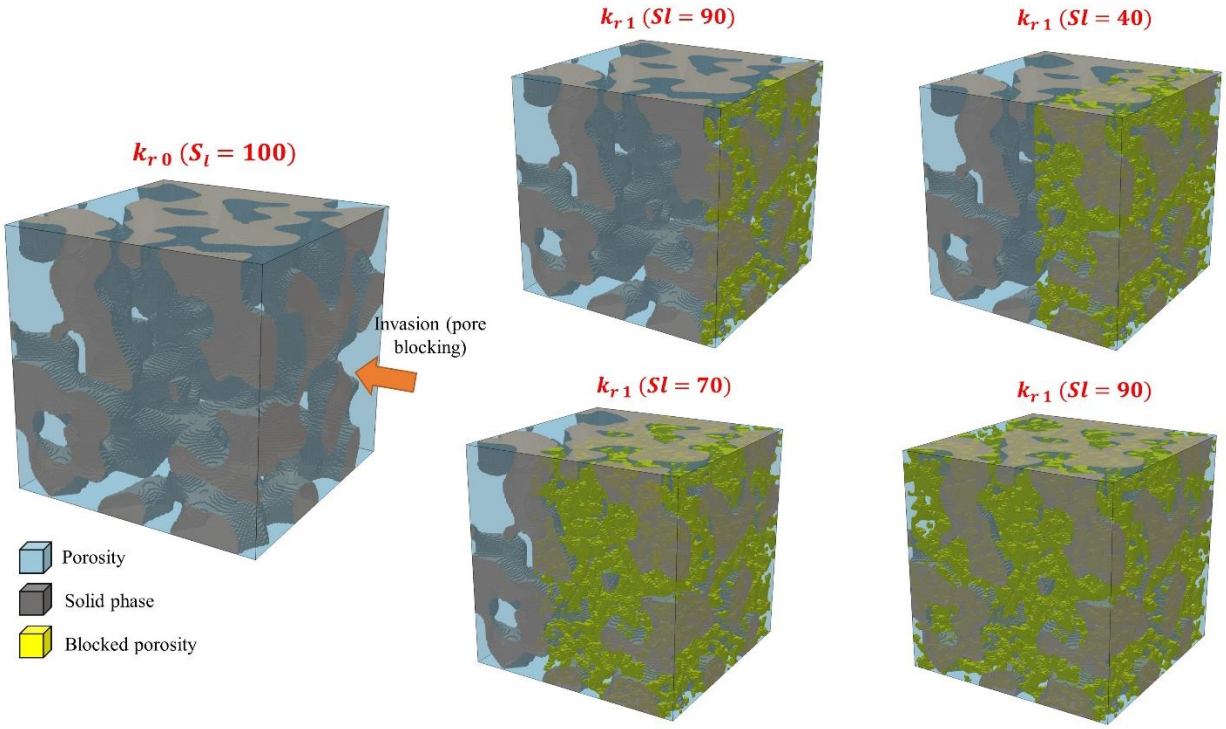

Figure 5. Sequential invasion of the network and calculating the relative permeability for each sequence (4 different degree of saturations).

4 Results and validation

The method proposed in this paper is validated against an extensive number of experiments available in literature. The validation is conducted in two parts: (i) intrinsic and (ii) unsaturated permeability. Table 1 shows the experimental details of each dataset. Note that the measured value for intrinsic permeability may differ depending on the experimental approach [2], [5], [37] and it can vary up to an order of magnitude and even higher[2], [5]. That is why an estimation within a range of order of magnitude is still seen as acceptable in this study. In addition to measurement uncertainties, there can be back calculation error effect involved in reported values, for example, when the permeability is back calculated using Van Genuchten [38]retention curve but the fitting is not perfect.

Table 1. Experimental data from literature [1]–[3], [5], [22]–[27]. *HCP: Hardened cement paste*

Material	Author	Measurement method	Material Type	W/C	Age (days)	Curing	Intrinsic permeability (m^2)
CP1	Baroghel-Bouny (1999)	Inverse analysis from mass loss	CEM I - HCP	0.34	365	Sealed then vacuum rewetted	10^{-21}
CP2	Ai et al (2001)	Thermo-permeametry	CEM I + 6% silica fume - HCP	0.4	548	Sealed and moist cured for 24 h then cured underwater	8.65×10^{-22}
CP3	Ye (2005)	Pressure cell	CEM I - HCP	0.4	28	Sealed then vacuum rewetted	9×10^{-22}
CP4				0.5			1.33×10^{-19}
CP5				0.6			1.82×10^{-18}
CP6	Grasley (2007)	Dynamic pressurization (DP)	CEM I - HCP	0.5	80	Limewater	3×10^{-21}
CP7				0.6	32		6.5×10^{-21}
CP8	Phung (2013)	Constant flow	CEM I - HCP	0.4	28	Limewater	8×10^{-21}
CP9				0.5			3×10^{-20}
CP10				0.6			7×10^{-20}
CP11	Kumar (2014)	MIP	CEM I - HCP	0.45	28	sealed	4×10^{-21}
CP12				0.5			1×10^{-20}

CP13				0.64			2×10^{-19}
CP14	Zamani (2014)	Inverse analysis	CEM I - HCP	0.4	28	Under water	4×10^{-21}
CP15	Egan (2017)	Inverse analysis	CEM I - HCP	0.45	56	Limewater	3×10^{-21}
CP16				0.55			6×10^{-21}
CP17				0.65			2×10^{-20}
CP18	Zhang (2018)	Beam Bending - Sorptivity	CEM I - HCP	0.5	365	Limewater	Avg.= 1.2×10^{-19}

313

4.1 Intrinsic permeability

The estimation of permeability involves carrying out microstructural modelling (hydration calculations) using the cement composition data reported by various researchers (OPC, CEM I here, only CP2 includes 6% silica fume). The results from the microstructural model is presented in Table 2, based on which pore network is constructed for each material composition, which is subsequently taken forward to estimate permeability. Note that to simulate permeability, 18 pore networks have been constructed corresponding to the 18 data sets available in Table 2. Table 2 also reports the intrinsic permeability measured in all three directions for each individual material, denoted as k_{0xx}, k_{0yy} *and* k_{0zz}. The results show that the k_0 values in different directions do not vary more than 3% indicating the representativeness of the network generated. A comparison of results from the proposed method against experimental observations are presented in Figure 6.

Table 2. The microstructure information of the studied materials.

Material	C3S (wt%)	C2S (wt%)	C3A (wt%)	C4AF (wt%)	W/C (wt%)	C-S-H (vol%)	LD C-S-H (vol%)	HD C-S-H (vol%)	Capillary Porosity (vol%)	Total Porosity (vol%)	Estimated Permeability (m^2) – k_0	Average Estimated Permeability (m^2) – k_0
CP1	57.28	23.98	3.03	7.59	0.34	0.50	0.18	0.32	0.12	0.24	$k_{0xx}=8.59\times10^{-22}$ $k_{0yy}=8.38\times10^{-22}$ $k_{0zz}=8.55\times10^{-22}$	8.51×10^{-22}
CP2	67.1	17.5	7.7	7.6	0.4	0.47	0.22	0.25	0.13	0.25	$k_{0xx}=1.29\times10^{-21}$ $k_{0yy}=1.25\times10^{-21}$ $k_{0zz}=1.26\times10^{-21}$	1.27×10^{-21}
CP3	63	13	8	9	0.4	0.47	0.22	0.25	0.14	0.25	$k_{0xx}=4.08\times10^{-21}$ $k_{0yy}=3.97\times10^{-21}$ $k_{0zz}=3.95\times10^{-21}$	4.00×10^{-21}
CP4					0.5	0.46	0.33	0.13	0.19	0.29	$k_{0xx}=2.17\times10^{-20}$ $k_{0yy}=2.22\times10^{-20}$ $k_{0zz}=2.23\times10^{-20}$	2.21×10^{-20}
CP5					0.6	0.46	0.37	0.09	0.23	0.33	$k_{0xx}=4.65\times10^{-19}$ $k_{0yy}=4.69\times10^{-19}$ $k_{0zz}=4.81\times10^{-19}$	4.72×10^{-19}
CP6	48.3	21.5	7.6	9.1	0.5	0.47	0.33	0.14	0.19	0.30	$k_{0xx}=1.91\times10^{-21}$ $k_{0yy}=1.93\times10^{-21}$ $k_{0zz}=1.97\times10^{-21}$	1.94×10^{-21}
CP7					0.6	0.46	0.36	0.10	0.22	0.32	$k_{0xx}=7.89\times10^{-20}$ $k_{0yy}=7.93\times10^{-20}$	7.86×10^{-20}

											$k_{0zz}=7.75\times10^{-20}$	
CP8	62.5	18	9	10	0.4	0.44	0.21	0.23	0.14	0.25	$k_{0xx}=4.41\times10^{-21}$ $k_{0yy}=4.53\times10^{-21}$ $k_{0zz}=4.39\times10^{-21}$	4.45×10^{-21}
CP9					0.5	0.44	0.32	0.12	0.19	0.30	$k_{0xx}=2.80\times10^{-20}$ $k_{0yy}=2.71\times10^{-20}$ $k_{0zz}=2.73\times10^{-20}$	2.75×10^{-20}
CP10					0.6	0.45	0.40	0.05	0.24	0.34	$k_{0xx}=1.18\times10^{-19}$ $k_{0yy}=1.15\times10^{-19}$ $k_{0zz}=1.17\times10^{-19}$	1.17×10^{-19}
CP11	59.2	16.7	9	10.3	0.45	0.49	0.29	0.20	0.18	0.29	$k_{0xx}=1.11\times10^{-20}$ $k_{0yy}=1.12\times10^{-20}$ $k_{0zz}=1.15\times10^{-20}$	1.13×10^{-20}
CP12					0.5	0.49	0.35	0.14	0.20	0.32	$k_{0xx}=2.58\times10^{-20}$ $k_{0yy}=2.49\times10^{-20}$ $k_{0zz}=2.51\times10^{-20}$	2.53×10^{-20}
CP13					0.64	0.46	0.40	0.06	0.27	0.37	$k_{0xx}=6.29\times10^{-19}$ $k_{0yy}=6.45\times10^{-19}$ $k_{0zz}=6.42\times10^{-19}$	6.39×10^{-19}
CP14	66.9	20	3.5	4.4	0.4	0.52	0.25	0.27	0.14	0.27	$k_{0xx}=2.29\times10^{-21}$ $k_{0yy}=2.38\times10^{-21}$ $k_{0zz}=2.30\times10^{-21}$	2.33×10^{-21}
CP15	56.5	18	6.3	11.4	0.45	0.46	0.28	0.18	0.17	0.28	$k_{0xx}=1.08\times10^{-20}$ $k_{0yy}=1.14\times10^{-20}$ $k_{0zz}=1.10\times10^{-20}$	1.11×10^{-20}

CP16					0.55	0.45	0.38	0.07	0.22	0.32	$k_{0xx}=5.31\times10^{-20}$ $k_{0yy}=5.45\times10^{-20}$ $k_{0zz}=5.42\times10^{-20}$	5.40×10^{-20}
CP17					0.65	0.44	0.38	0.06	0.26	0.36	$k_{0xx}=4.25\times10^{-19}$ $k_{0yy}=4.29\times10^{-19}$ $k_{0zz}=4.21\times10^{-19}$	4.25×10^{-19}
CP18	53.6	17.5	7.5	8.8	0.5	0.46	0.33	0.13	0.19	0.29	$k_{0xx}=2.74\times10^{-20}$ $k_{0yy}=2.67\times10^{-20}$ $k_{0zz}=2.73\times10^{-20}$	2.72×10^{-20}

327

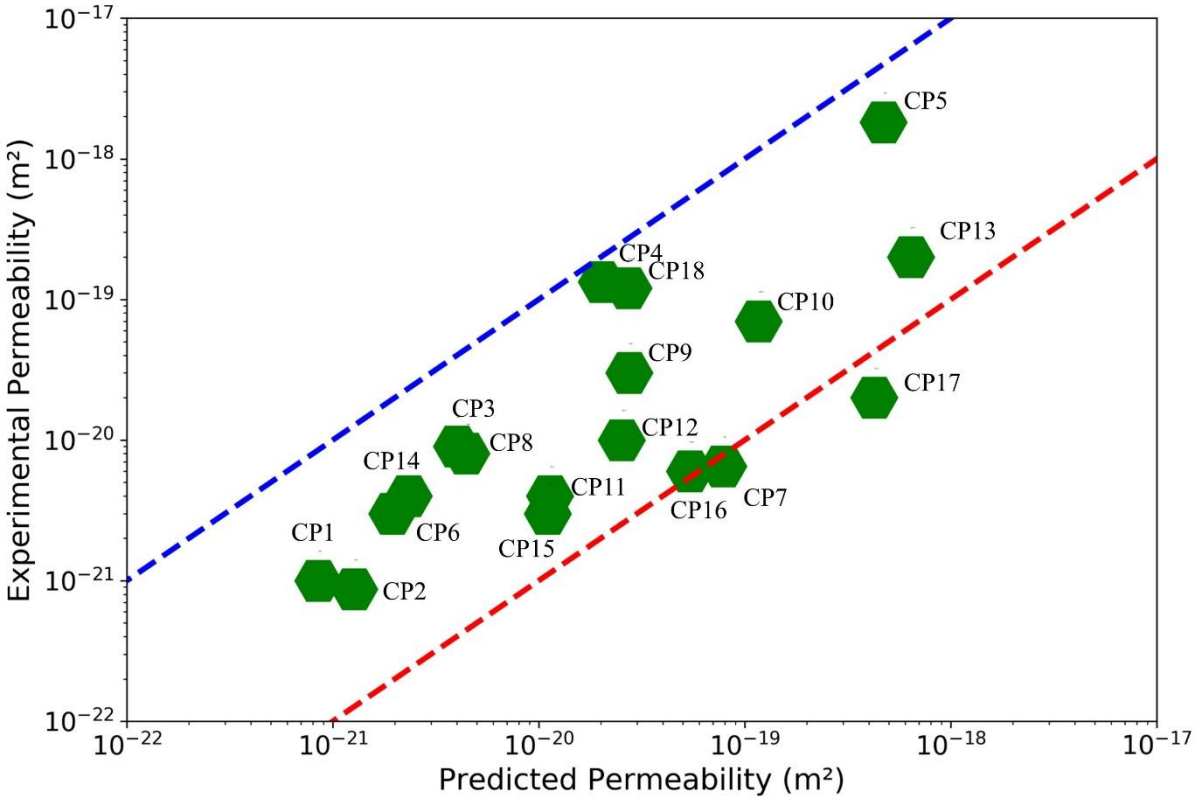

Figure 6. Estimated values using pore network modelling vs. experimental observations (dash lines order of magnitude lines).

Overall, the model results show a very good correspondence with the experimental observations. In fact, the results fall well within the same order of magnitude for 17 out of 18 studied cases. This confirms that the proposed model can successfully and systematically transfer information from microstructure into a pore network, which is representative of permeability of HCP.

The predicted value for CP17 is the only case where the model fails to estimate within the same order of magnitude as the experimentally observed value. However, in this case, the permeability is indirectly measured; firstly fitting a Van Genuchten [38] curve on experimental retention curve and then back calculating the mass loss using the fitted Van Genuchten curve. This method however is sensitive to fitting parameters of the retention curve and thus can be

affected by the accuracy of fitting. Moreover, different types of measurements can lead to different results and this is mainly due to experimental uncertainties. For instance, CP13 and CP17 have a relatively similar composition but the measured permeability for CP13 is exactly one order of magnitude less than that of CP17, while ratio of their permeability estimated by the proposed model is 3. The same argument holds for CP16, whose permeability value lies just at the border of the order of magnitude line.

The experimentally measured value for CP7, which is an OPC with W/C of 0.6 is 6.5×10^{-21} m^2 that is at least an order of magnitude lower than similar compositions with the same W/C ratio (CP5, CP10) and using different experimental methods. As already mentioned, the measurement method can also affect the measured value and this seems to be the case here. Furthermore, the estimated values using pore network seems to be mostly close to the values measured by constant flow and indirect measurements (inverse analysis).

In terms of improved accuracy the accuracy of proposed methodology compared to previous studies that targeted modelling the same variables, using comparable tools [9], [10], [14], [21] is considerably more e.g., in [10] the permeability of CP3-CP5 were (over)estimated in range of 10^{-16} -10^{-14} as opposed to 10^{-21} -10^{-19} in this study.

From the microstructural modelling results presented in Table 2, it is seen that the permeability can be correlated with the ratio of HD and LD C-S-H at C-S-H level and the capillary porosity at microstructure level. A parametric analysis (Figure 7) shows that for the study cases the permeability is directly proportional to the capillary porosity (*Figure 7* (a)) and inversely proportional to the HD C-S-H gel porosity (*Figure 7* (b)), which is the lowest permeable phase of C-S-H. In terms of comparative parameters, consistent trends for $V_{LD\,C\text{-}S\text{-}H}/V_{HD\,C\text{-}S\text{-}H}$ (*Figure 7* (c)) and $V_{capillary}/V_{total\,porosity}$ ratios (*Figure 7* (d)) are also observed (V_i denotes volume fraction

of phase i). The R^2 values sort the correlation of the parameters and permeability in the order of capillary porosity with R^2=0.82, capillary/total porosity with R^2=0.79 and $V_{LD\ C\text{-}S\text{-}H}$ /$V_{HD\ C\text{-}S\text{-}H}$ with R^2=0.64. The parametric analysis also shows that both capillary porosity (which is present in level-2) and C-S-H gel content (level-1) are important and contributing to the transport in hardened cement paste. While what has been concluded here is valid for mature pastes i.e., older than 28 days, it has been reported that at early age (1-10 days) the capillary porosity plays a more important role in permeability compared to the gel porosity. This is to be expected at early age due to higher connectivity of capillary pore space and lower degrees of hydration, which translates to coarser pore space [9], [24], [39], [40].

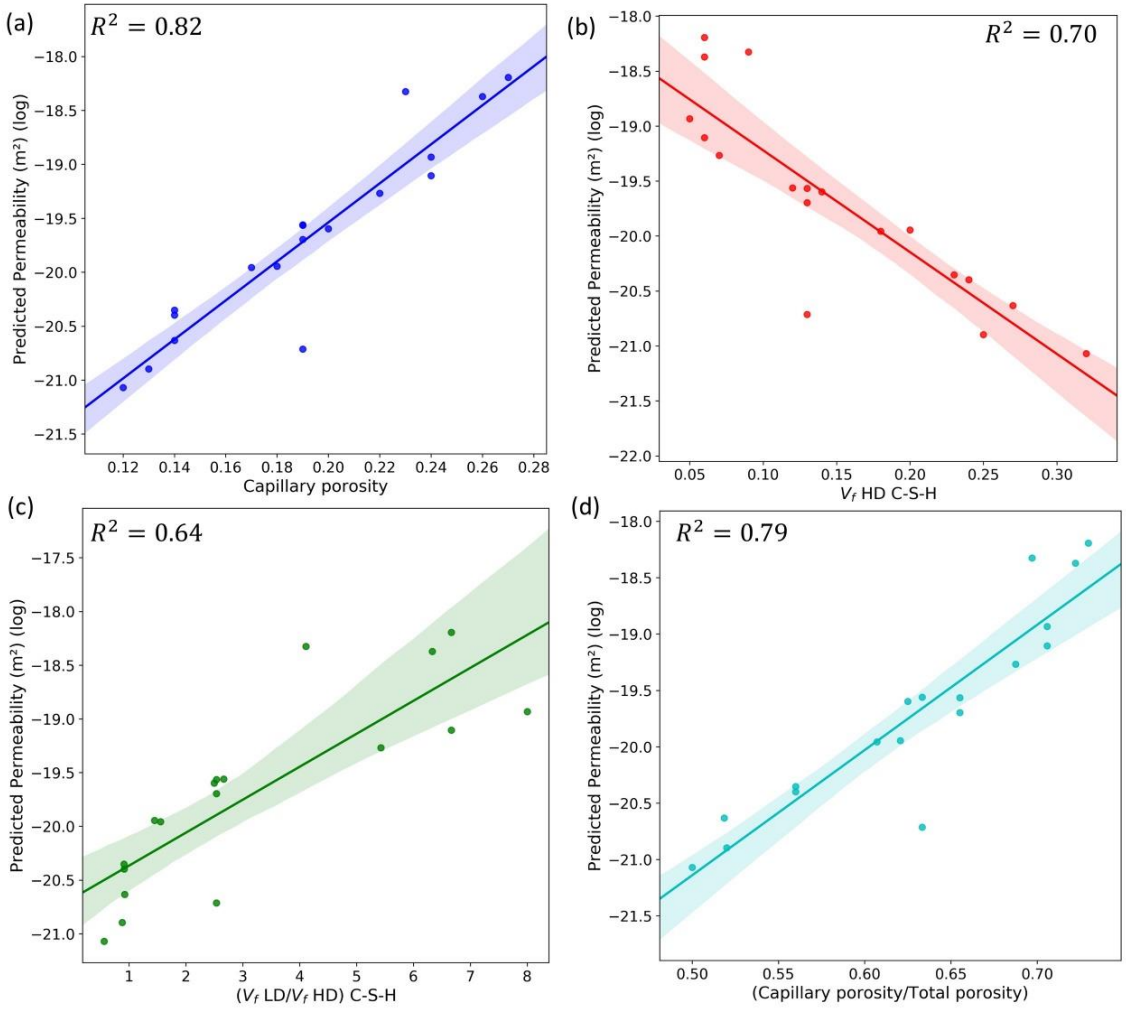

374

375 *Figure 7. Parametric analysis of intrinsic permeability for the studied materials.*

4.2 Unsaturated permeability

For the material CP1 and CP18 the unsaturated permeability values are available based on the inverse analysis, which will be used for comparisons. Additionally, comparisons will be made against the unsaturated permeability obtained from a calibrated water retention curve using the well-known Van Genuchten [38] model.

The Van Genuchten model for retention curve and unsaturated permeability are defined as follows:

$$S_l = \left[\left(\left(\frac{p_c}{a_{mu}}\right)^{\frac{b_{mu}}{b_{mu}-1}} + 1\right)^{-\frac{1}{b_{mu}}}\right] \quad (8)$$

where a_{mu} and b_{mu} are fitting parameters, which require fitting for each set of water sorption experiments available for the materials CP1 and CP18.

The unsaturated permeability is defined as:

$$k_l = k_0 k_{rl}(S_l) \quad (9)$$

where k_0 is the intrinsic permeability for CP1 and CP18 (Table 2) and $k_{rl}(S_l)$ is the relative permeability defined as :

$$k_{rl} = {S_l}^{0.5}\left[\left(1 - \left(1 - {S_l}^{b_{mu}}\right)^{\frac{1}{b_{mu}}}\right)^2\right] \quad (10)$$

Figure 8 shows a comparison of the results of the pore network model and the Van Genuchten model and the experimental data from the mass loss experiments for the materials CP1 and CP18. For both materials, the pore network model is more accurate than the Van Genuchten model. This proves not only that the network is representative for intrinsic permeability

simulation, but also for unsaturated scenarios where the constructed network can provide better results compared to the classical models. The advantage of the proposed framework lies in the fact that it contains more information and relevance from the material, while such relevance and link is missing in case of empirical models. Note that the experimental trend for CP1 is unreliable because it shows that the unsaturated permeability is higher at lower degrees of saturation. This is likely to be caused by experimental uncertainties [2], [5], [25].

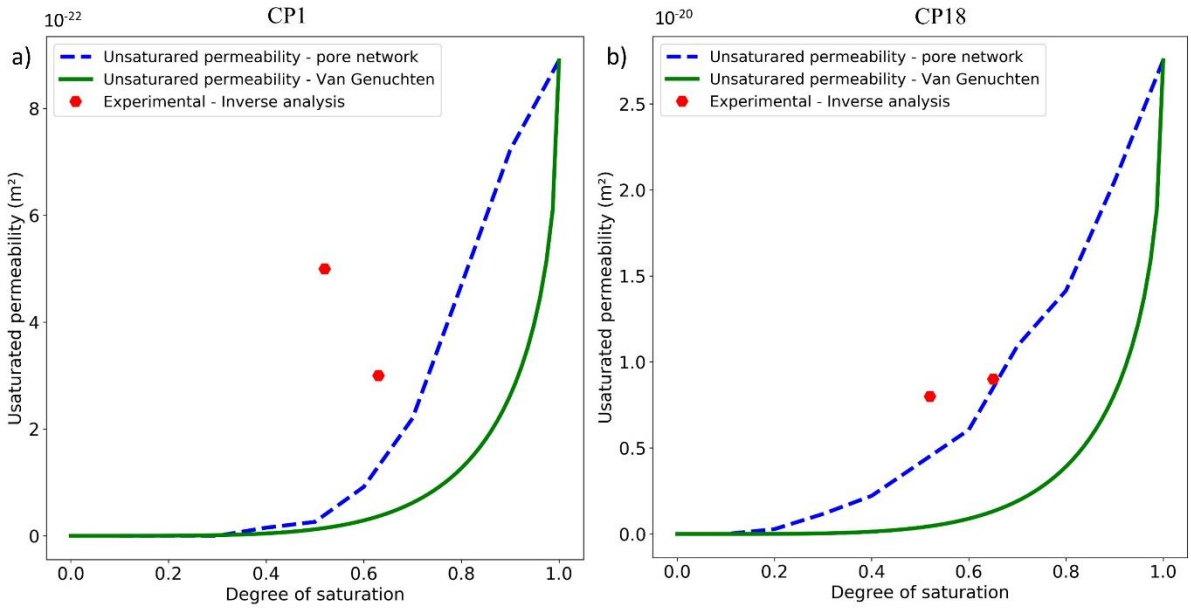

Figure 8. Unsaturated permeability estimated using pore network VS. experimental measurements

It is also worth noting that the unsaturated permeability estimated by pore network as well as the experimentally measured values roughly remain in the same order of magnitude of the intrinsic permeability up to *RH*=0.5. At this *RH*, pores with size of approximately 12 nm are desaturated. Pores smaller than 12 nm are mostly small capillary pores and gel pores. This indicates that gel pores are also contributing to the flow, even though because of their size they are weakly permeable, and their contribution is definitely not negligible as was suggested in [13], [16]. One additional conclusion to be drawn is that up to 50% *RH* the water permeability would still be in the range of intrinsic permeability indicating that moisture flow in the liquid

phase is the major mechanism in this range as argued previously by multiple authors, to mention a few [2], [5], [25], [41]. In other words, no two phase flow model is necessary to model moisture flow in unsaturated cement paste up to this *RH* level.

5 Conclusions

This study presents a new and fundamentally predictive methodology for computation of intrinsic and unsaturated permeability of OPC-based cementitious materials. The proposed methodology utilizes a multiscale numerical framework starting from cement composition and its microstructure to constructing a hierarchical pore network and computation of the permeability. Moreover, a novel multi-algorithmic approach is developed to compute unsaturated permeability at different degrees of saturation. This framework adopts different modeling tools including (i) particle packing for modelling the pore size distribution of the C-S-H gel pores, (ii) microstructural modelling to model hydration reaction kinetics, and (iii) pore network modelling. The microstructure is modelled using VCCTL software and pore network modelling used here is a customized version of OpenPNM [42] developed in python using mainly NumPy [43] and SciPy[44], [45] libraries. A quasi-static analysis of the network using Hagen–Poiseuille coupled with Young-Laplace equation (in a form of invasion algorithm [36]) is then invoked in pore bodies and throats to estimate saturated and unsaturated permeability, the Young-Laplace equation because the invasion algorithm resembles the drying by invading and blocking pores and throats.

The proposed approach is validated against eighteen different experiments available in the literature and obtained results are remarkably promising, indicating the flexibility and reliability of the framework. Additionally, a parametric analysis on dependency of intrinsic water permeability on microstructural variables such as capillary porosity, volume fraction of HD C-S-H etc., showed that the permeability can be correlated to the variables from both the level-1 (C-S-H gel level) and level-2 (capillary porosity). Finally, it was also observed that the proposed model can provide a more accurate results compared to Van Genuchten for unsaturated water permeability.

In terms of disadvantage of the proposed framework, its reliance on microstructural modelling and all the initial inputs that are derived herewith could have a negative impact on the final estimation if the microstructure is not accurate in reporting the phase fractions. Secondly, the applicability of the framework on blended cement systems is not investigated because of the lack of established microstructural modelling for these materials. However, CP2 in the studied materials includes 6% silica fume and estimated permeability is also fairly accurate. But applicability on systems with high percentage of additives such as limestone calcined cement [46], [47] remains uncertain. Finally, the proposed model is intended to operate at microstructural level with RVE size of few 100s of micrometers with no consideration of microcracks. Whereas in reality permeability experiments are carried out at centimeter scale and hence any effect of microcracks on permeability cannot be captured by this version of the model. However, this limitation can be easily overcome by adding synthetic microcracks into the RVE.

Acknowledgements

The first author gratefully acknowledges PhD sponsorship offered by SCK CEN. The findings and conclusions in this paper are those of the authors and do not represent the official position of SCK CEN. The authors are also grateful for insightful discussions with Dr. Tri Quoc Phung, and for the constructive criticisms of anonymous reviewers of this paper.

REFERENCES

[1] Q. T. Phung, N. Maes, G. De Schutter, D. Jacques, and G. Ye, "Determination of water permeability of cementitious materials using a controlled constant flow method," *Constr. Build. Mater.*, vol. 47, pp. 1488–1496, 2013, doi: https://doi.org/10.1016/j.conbuildmat.2013.06.074.

[2] Z. Zhang, M. Thiery, and V. Baroghel-Bouny, "Investigation of moisture transport properties of cementitious materials," *Cem. Concr. Res.*, vol. 89, pp. 257–268, 2016, doi: https://doi.org/10.1016/j.cemconres.2016.08.013.

[3] A. Kumar, S. Ketel, K. Vance, T. Oey, N. Neithalath, and G. Sant, "Water Vapor Sorption in Cementitious Materials—Measurement, Modeling and Interpretation," *Transp. Porous Media*, vol. 103, no. 1, pp. 69–98, 2014, doi: 10.1007/s11242-014-0288-5.

[4] Q. Xiong, T. G. Baychev, and A. P. Jivkov, "Review of pore network modelling of porous media: Experimental characterisations, network constructions and applications to reactive transport," *J. Contam. Hydrol.*, vol. 192, pp. 101–117, 2016, doi: https://doi.org/10.1016/j.jconhyd.2016.07.002.

[5] Z. Zhang and G. Scherer, "Determination of water permeability for a moisture transport model with minimized batch effect," *Constr. Build. Mater.*, vol. 191, pp. 193–205, 2018, doi: https://doi.org/10.1016/j.conbuildmat.2018.09.194.

[6] M. Kozeny, "Uber kapillare Leitung des Wassers im Boden," *Sitzber. Akad. Wiss. Wein, Math-naturw*, vol. 136, p. Abt. II a, P. 277, 1927.

[7] P. C. Carman, “Fluid flow through granular beds,” *Chem. Eng. Res. Des.*, vol. 75, pp. S32–S48, 1997, doi: https://doi.org/10.1016/S0263-8762(97)80003-2.

[8] A. J. Katz and A. H. Thompson, “Quantitative prediction of permeability in porous rock,” *Phys. Rev. B*, vol. 34, no. 11, pp. 8179–8181, Dec. 1986, doi: 10.1103/PhysRevB.34.8179.

[9] G. Ye, P. Lura, and K. van Breugel, “Modelling of water permeability in cementitious materials,” *Mater. Struct.*, vol. 39, no. 9, pp. 877–885, 2006, doi: 10.1617/s11527-006-9138-4.

[10] X. Li and Y. Xu, “Microstructure-Based Modeling for Water Permeability of Hydrating Cement Paste,” *J. Adv. Concr. Technol.*, vol. 17, no. 7, pp. 405–418, 2019, doi: 10.3151/jact.17.405.

[11] Y. Song, G. Dai, L. Zhao, Z. Bian, P. Li, and L. Song, “Permeability prediction of hydrated cement paste based on its 3D image analysis,” *Constr. Build. Mater.*, vol. 247, p. 118527, 2020, doi: https://doi.org/10.1016/j.conbuildmat.2020.118527.

[12] P. Yu, Y. H. Duan, E. Chen, S. W. Tang, and X. R. Wang, “Microstructure-based fractal models for heat and mass transport properties of cement paste,” *Int. J. Heat Mass Transf.*, vol. 126, pp. 432–447, 2018, doi: https://doi.org/10.1016/j.ijheatmasstransfer.2018.05.150.

[13] M. Zalzale, P. J. McDonald, and K. L. Scrivener, “A 3D lattice Boltzmann effective media study: understanding the role of C-S-H and water saturation on the permeability of cement paste,” *Model. Simul. Mater. Sci. Eng.*, vol. 21, no. 8, p. 85016, 2013, doi:

10.1088/0965-0393/21/8/085016.

[14] K. Li, P. Stroeven, and N. L. B. Le, “METHODOLOGY FOR POROSIMETRY IN VIRTUAL CEMENTITIOUS COMPOSITES TO ECONOMICALLY AND RELIABLY ESTIMATE PERMEABILITY,” *Image Anal. & Stereol. Vol 34, No 2 (2015)DO - 10.5566/ias.1271* , May 2015, [Online]. Available: https://www.ias-iss.org/ojs/IAS/article/view/1271.

[15] K. Li, “Numerical Determination of Permeability in Unsaturated Cementitious Materials,” Delft University of Technology, 2017.

[16] M. Zalzale and P. J. McDonald, “Lattice Boltzmann simulations of the permeability and capillary adsorption of cement model microstructures,” *Cem. Concr. Res.*, vol. 42, no. 12, pp. 1601–1610, 2012, doi: https://doi.org/10.1016/j.cemconres.2012.09.003.

[17] L. Ecay, D. Grégoire, and G. Pijaudier-Cabot, “On the prediction of permeability and relative permeability from pore size distributions,” *Cem. Concr. Res.*, vol. 133, p. 106074, 2020, doi: https://doi.org/10.1016/j.cemconres.2020.106074.

[18] K. Fadi, G. David, and P.-C. Gilles, “A Hierarchical Model for the Computation of Permeation Properties of Porous Materials and Their Enhancement due to Microcracks,” *J. Eng. Mech.*, vol. 144, no. 2, p. 4017160, Feb. 2018, doi: 10.1061/(ASCE)EM.1943-7889.0001392.

[19] G. Mason, “The effect of pore space connectivity on the hysteresis of capillary condensation in adsorption—desorption isotherms,” *J. Colloid Interface Sci.*, vol. 88, no. 1, pp. 36–46, 1982, doi: https://doi.org/10.1016/0021-9797(82)90153-9.

[20] G. Mason and D. H. Everett, “A model of adsorption-desorption hysteresis in which hysteresis is primarily developed by the interconnections in a network of pores,” *Proc. R. Soc. London. A. Math. Phys. Sci.*, vol. 390, no. 1798, pp. 47–72, Nov. 1983, doi: 10.1098/rspa.1983.0122.

[21] K. Li, L. Xu, P. Stroeven, and C. Shi, “Water permeability of unsaturated cementitious materials: A review,” *Constr. Build. Mater.*, vol. 302, p. 124168, 2021, doi: https://doi.org/10.1016/j.conbuildmat.2021.124168.

[22] Z. C. Grasley, G. W. Scherer, D. A. Lange, and J. J. Valenza, “Dynamic pressurization method for measuring permeability and modulus: II. cementitious materials,” *Mater. Struct.*, vol. 40, no. 7, pp. 711–721, 2007, doi: 10.1617/s11527-006-9184-y.

[23] H. Ai, J. F. Young, and G. W. Scherer, “Thermal Expansion Kinetics: Method to Measure Permeability of Cementitious Materials: II, Application to Hardened Cement Pastes,” *J. Am. Ceram. Soc.*, vol. 84, no. 2, pp. 385–391, Feb. 2001, doi: https://doi.org/10.1111/j.1151-2916.2001.tb00666.x.

[24] G. Ye, “Percolation of capillary pores in hardening cement pastes,” *Cem. Concr. Res.*, vol. 35, no. 1, pp. 167–176, 2005, doi: https://doi.org/10.1016/j.cemconres.2004.07.033.

[25] V. Baroghel-Bouny, M. Mainguy, T. Lassabatere, and O. Coussy, “Characterization and identification of equilibrium and transfer moisture properties for ordinary and high-performance cementitious materials,” *Cem. Concr. Res.*, vol. 29, no. 8, pp. 1225–1238, 1999, doi: https://doi.org/10.1016/S0008-8846(99)00102-7.

[26] S. Zamani, R. M. Kowalczyk, and P. J. McDonald, “The relative humidity dependence of the permeability of cement paste measured using GARField NMR profiling,” *Cem. Concr. Res.*, vol. 57, pp. 88–94, 2014, doi: https://doi.org/10.1016/j.cemconres.2013.12.010.

[27] G. Egan, A. Kumar, N. Neithalath, and G. Sant, “Re-examining the influence of the inclusion characteristics on the drying shrinkage of cementitious composites,” *Constr. Build. Mater.*, vol. 146, pp. 713–722, 2017, doi: https://doi.org/10.1016/j.conbuildmat.2017.04.048.

[28] S. Babaei, S. C. Seetharam, U. Muehlich, A. Dizier, G. Steenackers, and B. Craeye, “A multiscale framework to estimate water sorption isotherms for OPC-based materials,” *Cem. Concr. Compos.*, vol. 105, p. 103415, 2020, doi: https://doi.org/10.1016/j.cemconcomp.2019.103415.

[29] J. Bullard, “Virtual Cement and Concrete Testing Laboratory: Version 9.5 User Guide.” Special Publication (NIST SP), National Institute of Standards and Technology, Gaithersburg, MD, 2014.

[30] S. Babaei, *A multiscale approach to model thermo-hydro-mechanical behaviour of nonreinforced concrete* . Antwerp: University of Antwerp, Faculty of Applied Engineering, 2021.

[31] S. Babaei, S. C. Seetharam, A. Dizier, G. Steenackers, and B. Craeye, “An analytical framework for estimating drying shrinkage strain of OPC based hardened cement paste,” *Cem. Concr. Compos.*, vol. 115, p. 103833, 2021, doi: https://doi.org/10.1016/j.cemconcomp.2020.103833.

[32] D. P. Bentz, “Three-Dimensional Computer Simulation of Portland Cement Hydration and Microstructure Development,” *J. Am. Ceram. Soc.*, vol. 80, no. 1, pp. 3–21, Jan. 1997, doi: https://doi.org/10.1111/j.1151-2916.1997.tb02785.x.

[33] T. C. POWERS, “Structure and Physical Properties of Hardened Portland Cement Paste,” *J. Am. Ceram. Soc.*, vol. 41, no. 1, pp. 1–6, Jan. 1958, doi: https://doi.org/10.1111/j.1151-2916.1958.tb13494.x.

[34] M. Akbari, D. Sinton, and M. Bahrami, “Viscous flow in variable cross-section microchannels of arbitrary shapes,” *Int. J. Heat Mass Transf.*, vol. 54, no. 17, pp. 3970–3978, 2011, doi: https://doi.org/10.1016/j.ijheatmasstransfer.2011.04.028.

[35] M. Islahuddin and H. Janssen, “Hygric property estimation of porous building materials with multiscale pore structures,” *Energy Procedia*, vol. 132, pp. 273–278, 2017, doi: https://doi.org/10.1016/j.egypro.2017.09.722.

[36] D. Wilkinson and J. F. Willemsen, “Invasion percolation: a new form of percolation theory,” *J. Phys. A. Math. Gen.*, vol. 16, no. 14, pp. 3365–3376, 1983, doi: 10.1088/0305-4470/16/14/028.

[37] S. Goto and D. M. Roy, “The effect of w/c ratio and curing temperature on the permeability of hardened cement paste,” *Cem. Concr. Res.*, vol. 11, no. 4, pp. 575–579, 1981, doi: https://doi.org/10.1016/0008-8846(81)90087-9.

[38] M. T. van Genuchten, “A Closed-form Equation for Predicting the Hydraulic Conductivity of Unsaturated Soils,” *Soil Sci. Soc. Am. J.*, vol. 44, no. 5, pp. 892–898, Sep. 1980, doi: https://doi.org/10.2136/sssaj1980.03615995004400050002x.

[39] M. Zhang, “Pore-scale modelling of relative permeability of cementitious materials using X-ray computed microtomography images,” *Cem. Concr. Res.*, vol. 95, pp. 18–29, 2017, doi: https://doi.org/10.1016/j.cemconres.2017.02.005.

[40] M. Bogdan, “Morphological multisscale modeling of cementitious materials -- Application to effective diffusive properties prediction,” École normale supérieure de Cachan - ENS Cachan, 2015.

[41] V. Baroghel-Bouny, “Water vapour sorption experiments on hardened cementitious materials: Part I: Essential tool for analysis of hygral behaviour and its relation to pore structure,” *Cem. Concr. Res.*, vol. 37, no. 3, pp. 414–437, 2007, doi: https://doi.org/10.1016/j.cemconres.2006.11.019.

[42] J. Gostick *et al.*, “OpenPNM: A Pore Network Modeling Package,” *Comput. Sci. Eng.*, vol. 18, no. 4, pp. 60–74, 2016, doi: 10.1109/MCSE.2016.49.

[43] C. R. Harris *et al.*, “Array programming with NumPy,” *Nature*, vol. 585, no. 7825, pp. 357–362, 2020, doi: 10.1038/s41586-020-2649-2.

[44] P. Virtanen *et al.*, “SciPy 1.0: fundamental algorithms for scientific computing in Python,” *Nat. Methods*, vol. 17, no. 3, pp. 261–272, Mar. 2020, doi: 10.1038/s41592-019-0686-2.

[45] S. van der Walt *et al.*, “scikit-image: image processing in Python,” *PeerJ*, vol. 2, p. e453, 2014, doi: 10.7717/peerj.453.

[46] K. L. Scrivener, V. M. John, and E. M. Gartner, “Eco-efficient cements: Potential economically viable solutions for a low-CO2 cement-based materials industry,” *Cem.*

Concr. Res., vol. 114, pp. 2–26, 2018, doi: https://doi.org/10.1016/j.cemconres.2018.03.015.

[47] W. Wilson, L. Sorelli, and A. Tagnit-Hamou, "Unveiling micro-chemo-mechanical properties of C–(A)–S–H and other phases in blended-cement pastes," *Cem. Concr. Res.*, vol. 107, pp. 317–336, 2018, doi: https://doi.org/10.1016/j.cemconres.2018.02.010.

Response to Reviewers

Authors would like to thank reviewers and editor for their time and helping improving the manuscript.

Reviewer 2

Reviewer #2: Most of the improvements have been made to the reviewers' suggestions. However, some existing studies have compared experimental and predicted results. Please describe how much the accuracy has improved compared to that.

The modelling framework presented in this study is validated against a wide range of experimental observation reported in Table. 2 and Figure. 6-7. In terms of improved accuracy as mentioned in lines 70-100 the accuracy of proposed methodology compared to previous studies that targeted modelling the same variables, is considerably more, to mention a few [1]–[4]. The main reason is that this study takes a wider range of pore size distribution into account compared to the majority of the studies. One additional feature in this study is the implementation of multiple algorithms on a multiscale network. It is also worth mentioning that most of the experimental data studied in this research are purely experimental studies. Therefore, benchmarking is not feasible. Nevertheless a short explanation is added to text to point this more clearly out, line 353-356.

References:

[1] X. Li and Y. Xu, “Microstructure-Based Modeling for Water Permeability of Hydrating Cement Paste,” *J. Adv. Concr. Technol.*, vol. 17, no. 7, pp. 405–418, 2019, doi: 10.3151/jact.17.405.

[2] G. Ye, P. Lura, and K. van Breugel, “Modelling of water permeability in cementitious materials,” *Mater. Struct.*, vol. 39, no. 9, pp. 877–885, 2006, doi: 10.1617/s11527-006-9138-4.

[3] K. Li, P. Stroeven, and N. L. B. Le, “METHODOLOGY FOR POROSIMETRY IN VIRTUAL CEMENTITIOUS COMPOSITES TO ECONOMICALLY AND RELIABLY ESTIMATE PERMEABILITY,” *Image Anal. & Stereol. Vol 34, No 2 (2015)DO - 10.5566/ias.1271* , May 2015, [Online]. Available: https://www.ias-iss.org/ojs/IAS/article/view/1271.

[4] K. Li, L. Xu, P. Stroeven, and C. Shi, “Water permeability of unsaturated cementitious materials: A review,” *Constr. Build. Mater.*, vol. 302, p. 124168, 2021, doi: https://doi.org/10.1016/j.conbuildmat.2021.124168.

- A multiscale modelling framework for permeability of cementitious materials is proposed
- The framework relies on: particle packing, cement hydration and a pore network model
- The proposed model takes the contribution of all the pore classes into account
- A new method for simulation of unsaturated permeability is introduced
- The proposed model is extensively validated and results are discussed in details

Saeid Babaei: Conceptualization, Methodology, Simulations, Data collection, Original Draft Writing- Reviewing and Editing, Visualization. **Suresh Seetharam**: Writing- Reviewing and Editing, Supervision. **Arnaud Dizier:** Supervision. **Gunther Steenackers:** Supervision. **Bart Craeye:** Conceptualization, Writing- Reviewing and Editing, Supervision.

Permeability of Cementitious Materials using a Multiscale Pore Network Model

Saeid Babaei* [(1)a,b,c], Suresh C. Seetharam [(2)b], Arnaud Dizier[(3)d], Gunther Steenackers[(4)c,e] and Bart Craeye[(5)c,f]

[a] SVK N.V., Aerschotstraat 114 B-9100 Sint-Niklaas, Belgium.

[b] Engineered and Geosystems Analysis Unit, Institute for Environment, Health, and Safety, Belgian Nuclear Research Centre (SCK•CEN), Boeretang 200, B-2400 Mol, Belgium.

[c] Faculty of Applied Engineering, University of Antwerp, EMIB Research Group, Groenenborgerlaan 171 - 2020 Antwerpen , Belgium.

[d] EIG, EURIDICE, Belgian Nuclear Research Centre (SCK•CEN), Boeretang 200, B-2400 Mol, Belgium.

[e] Faculty of Applied Engineering, University of Antwerp | Op3Mech Research Group Groenenborgerlaan 171 - 2020 Antwerpen.

[f] Odisse University College, Industrial Services & Technologies, DUBIT Research Unit, Belgium.

(1) Tel: +32 474740440, saeid.babaei@svk.be; saeid.babaei@uantwerpen.be

(2) Tel: +32 14 333208, suresh.seetharam@sckcen.be

(3) Tel: +32 14 332998, arnaud.dizier@euridice.be

(4) Tel: +32 00 000000, gunther.steenackers@uantwerpen.be

(5) Tel: +32 00 000000, bart.craeye@uantwerpen.be

Declaration of interests

☒ The authors declare that they have no known competing financial interests or personal relationships that could have appeared to influence the work reported in this paper.

☐The authors declare the following financial interests/personal relationships which may be considered as potential competing interests: